Comparative Whole-Brain Mapping of Isoflurane and Ketamine-Activated Nuclei and Functional Networks

Keywords: c-Fos; Isoflurane; Ketamine; Functional network.

Abstract

Ketamine (KET) and isoflurane (ISO) are two widely used general anesthetics, yet their distinct and shared neurophysiological mechanisms remain elusive. In this study, we conducted a comparative analysis of KET and ISO effects on c-Fos expression across the brain, utilizing principal component analysis (PCA) and c-Fos-based functional network analysis to evaluate the responses of individual brain regions to each anesthetic. Our findings demonstrate that KET significantly activates cortical and subcortical arousal-promoting nuclei, with the somatosensory cortex (SS) serving as a hub node, corroborating the top-down general anesthesia theory for dissociative anesthesia. In contrast, ISO activates the nuclei in the hypothalamus and brainstem, with the locus coeruleus (LC) as a hub node, implying a bottom-up mechanism for anesthetic-induced unconsciousness. Notably, the coactivation of sleep-wakefulness regulation, analgesia-related, neuroendocrine-related nuclei (e.g., prelimbic area (PL) and infralimbic areas (ILA), and the anterior paraventricular nucleus (aPVT), Edinger-Westphal nucleus (EW), locus coeruleus (LC), parabrachial nucleus (PB), solitary tract nucleus (NTS)) by both anesthetics underscores shared features such as unconsciousness, analgesia, and autonomic regulation, irrespective of their specific molecular targets. In conclusion, our results emphasize the distinct actions of KET and ISO while also uncovering the commonly activated brain regions, thus contributing to the advancement of our understanding of the mechanisms underlying general anesthesia.

Introduction

Despite considerable investigation into the molecular targets, neural circuits, and functional connectivity associated with various anesthetics, our comprehension of their effects on overall brain activity continues to be limited and incomplete [1]. At the molecular level, ketamine (KET) and isoflurane (ISO) interact with N-methyl-D-aspartate (NMDA) and gamma-aminobutyric acid type A (GABAa) receptors, respectively, modulating neuronal excitability and ultimately leading to a loss of consciousness [2]. In systems neuroscience,

the neural mechanisms of anesthetic induced unconsciousness involve both top-down and bottom-up processes [3, 4]. As evidenced by in vivo electrophysiology or functional magnetic resonance imaging (fMRI) studies, the top-down paradigm illustrates that anesthetics induce unconsciousness by disrupting corticocortical and corticothalamic circuits responsible for neural information integration, while peripheral sensory information can still be conveyed to the primary sensory cortex [5, 6]. The bottom-up approach, exemplified by ISO, involves the activation of sleep-promoting nuclei like ventral lateral preoptic nucleus (VLPO) and inhibition of arousal centers in the brainstem and diencephalon, supporting the shared circuits of sleep and anesthesia [7, 8]. However, the limited spatial resolution of fMRI studies and the inability of EEG to capture specific brainstem nuclei hinder the acquisition of comprehensive whole-brain information. Although a substantial body of knowledge has been amassed, our understanding of the reciprocal responses among different brain regions during general anesthesia remains relatively sparse and fragmented. To bridge these gaps, further investigation using advanced techniques that can capture the whole-brain dynamics is needed to elucidate the complex interactions and shared mechanisms between various anesthetics.

Neuronal extracellular stimulation typically results in the elevation of adenosine 3',5'-cyclic monophosphate (cAMP) levels and calcium influx, ultimately leading to the upregulation of immediate early genes (IEGs) such as c-fos [9, 10]. The translation product of c-fos, c-Fos protein, offers single-cell spatial resolution and has been utilized as a biomarker to identify anesthetic-activated brain regions [11]. Previous investigations of c-Fos expression throughout the brain demonstrated that GABAergic agents inhibited cortical activity while concurrently activating subcortical brain regions, including the VLPO, median preoptic nucleus (MnPO), lateral septal nucleus (LS), Edinger-Westphal nucleus (EW), and locus coeruleus (LC) [12-15]. In contrast, KET was shown to provoke wake-like c-Fos expression and intense augmentation of c-Fos expression in various brain regions at clinical dosages (75-100 mg/kg) [13]. It is important to note that these experiments administered KET at lights-on and GABAa receptor agonists at lights-off, potentially introducing circadian influences for direct comparison of ISO and KET. Moreover, it has been re-

vealed that state of general anesthesia is not determined by activity in individual brain areas, but emerges as a global change within the brain. This change involves the activation of lateral habenular nucleus (LHb), VLPO, supraoptic nucleus (SON), and central amygdaloid nucleus (CeA), which are essential for anesthetics induced sedation, unconsciousness, or analgesia [7, 16-18]. However, brain-wide mapping and comparison of distinct anesthetic (KET and ISO) activated nuclei at a cellular level have not been fully elucidated.

In this study, we examined the distribution of nuclei activated by ISO and KET in 987 brain regions using immunochemical labeling and a customized MATLAB software package, which facilitated signal detection and registration to the Allen Mouse Brain Atlas reference [19]. We compared whole-brain c-Fos expression induced by KET and ISO through principal component analysis (PCA) and calculated inter-regional correlations by determining the covariance across subjects for each brain region pair. We then extracted significantly positively correlated brain regions to construct functional networks and performed graph theory-based network analyses to identify hub nodes. Our results uncovered distinct yet overlapping whole-brain activation patterns for KET and ISO.

Results

A comparison of the activation patterns of c-Fos in 53 brain areas in response to ISO and KET

To examine the pattern of c-Fos expression throughout the brain, 1.5% ISO was continuously ventilated, or 100 mg/kg KET was administrated 90 minutes before harvesting (Figure 1A). Raw images of brain slices were aligned to the Allen Mouse Brain Atlas (Figure 1B). The entire brain was divided into 12 main regions in grade four with a total of 53 subregions in supplementary table 1. We first calculated the c-Fos cell density in each brain region across the four groups and then log-transformed the data for principal component analysis (PCA). The top two principal components revealed a clear separation between the KET and ISO groups, with KET induced c-Fos expression closely associated with PC1, accounting for 30.72% of the variance, while ISO was associated with PC2, accounting for 25.89%. The absence of overlap between PC1 and PC2 suggests distinct patterns of brain region activation for each anesthetic (Figure 2A). Figure 2B illustrates the

component coefficients of principal component 1 (PC1) and principal component 2 (PC2) for each brain region. The points in the figure represent brain regions with absolute component coefficients within the top 25%. KET, closely related to PC1, predominantly affected cortical regions, as evidenced by top 25% positive PC1 coefficients in MOB, AON, MO, ACA, and ORB, while subcortical areas exhibited negative coefficients. In contrast, ISO, showing a notable association with PC2, displayed top 25% positive coefficients in PALc, LSX of CNU , cortical ILA, and hypothalamic PVZ, with top 25% negative coefficients primarily found in cortical regions. These findings reveal distinct patterns of brain region activation for each anesthetic, with KET primarily affecting cortical regions, and ISO mainly influencing the central nucleus (CNU) and hypothalamus. To reduce inter-individual variability, we normalized c-Fos+ cell counts in each brain area by dividing them by the total c-Fos+ cells in the entire brain (Figure 2C), enabling a more accurate comparison of KET and SO induced activation patterns. In line with PCA results, KET significantly activated the isocortex (16.55 ± 2.31 vs. 40.13 ± 1.97, $P < 0.001$) and reduced the proportion of c-Fos+ cells in the hypothalamus (14.88 ± 2.18 vs. 4.03 ± 0.57, $P = 0.001$) and midbrain (21.87 ± 2.74 vs. 6.48 ± 1.06, $P = 0.001$) compared to the saline group. In contrast, ISO induced c-Fos+ cells were mainly observed in the striatum and hypothalamus compared to the home cage group, specifically in the periventricular zone (PVZ) (2.330 ± 0.759 vs. 6.63 ± 0.84, $P = 0.004$) and lateral zone (LZ) (2.82 ± 0.3 vs. 5.59 ± 0.75, $P = 0.007$) of the hypothalamus, as well as STRv (0.59 ± 0.10 vs. 2.77 ± 0.40, $P < 0.001$) and LSX (1.93 ± 0.59 vs. 5.11 ± 0.41, $P = 0.0012$) of the striatum (Figure 2C and Table 1). In summary, our findings reveal that KET predominantly affects cortical regions, whereas isoflurane mainly targets subcortical areas, specifically the striatum, and hypothalamus. These results demonstrate distinct patterns of brain region activation for each anesthetic agent.

Similarities and differences in ISO and KET activated c-Fos brain areas.

To further elucidate the similarities and differences between ISO and KET induced c-Fos expression patterns, we conducted a PCA on the logarithm of cell density across 201 brain regions, aiming to analyze their responses and characterize the variance among the respective experimental groups (Figure

3). The top two principal components displayed well-separated ISO and KET groups (Figure 3A), where the KET group had a strong association with PC1 (accounting for 28.97% of the variance) and the ISO group was associated with PC2 (accounting for 15.54% of the variance), indicating distinct features for the ISO and KET groups. We then further calculated the PC coefficients corresponding to the c-Fos density within each brain region (Figure 3B). The points in the figure represent brain regions with absolute component coefficients within the top 25%, highlighting the most influential regions in the PCA analysis. KET, closely associated with PC1, mainly activates brain regions within the cerebral cortex (CTX), including the visceral area (VISC), claustrum (CLA), dorsal peduncular area (DP), orbital area (ORB), and temporal association areas (TEA), while significantly inhibiting the hypothalamus, midbrain, and hindbrain. In contrast, ISO, closely associated with PC2, predominantly activates the hypothalamic regions, such as the ventrolateral preoptic nucleus (VLPO), suprachiasmatic nucleus (SCH), tuberal nucleus (TU), medial preoptic area (MPO), and supraoptic nucleus (SON), as well as certain nuclei in the central nucleus (CNU), while suppressing the cortex, midbrain, and hindbrain. KET predominantly affects brain regions within the cerebral cortex (CTX), while significantly inhibiting the hypothalamus, midbrain, and hindbrain. This result is in line with the top-down mechanism proposed previously, whereby anesthetic agents suppress consciousness by modulating cortical and thalamocortical circuits involved in the integration of neural information. ISO primarily activates hypothalamic regions, while suppressing the cortex, midbrain, and hindbrain. This aligns with the bottom-up mechanism, where anesthetics suppress consciousness by modulating sleep-wakefulness nuclei and neural circuits in the brainstem and diencephalon that have evolved to control arousal states[4]. We summarized the responses differences between the two anesthetics in Figure 3C, KET acts mainly via the top down mechanism, affecting cortical regions, while ISO operates through the bottom up mechanism, primarily targeting subcortical areas such as the hypothalamus, suggesting that different anesthetic agents may achieve the loss of consciousness by modulating distinct brain regions and neural circuits.

Identifying brain regions activated by KET

We further employed quantitative methods to identify the brain regions activated by KET across the entire brain. Our findings concur with previous studies, numerous cortical regions associated with somatosensory, auditory, visual, and movement were activated (Figure 4A and C, Supplementary Figure 1, Supplementary Table 2). Additionally, we identified several innovative observations that enrich the current understanding in this field. To provide a clearer overview of our findings, we categorized the activated brain areas based on their functions: (1) Arousal: Several nuclei associated with arousal were activated, including the prelimbic area (PL), infralimbic cortex (ILA), paraventricular nucleus of the thalamus (PVT), sublaterodorsal nucleus (SLD), and dorsal raphe (DR). Prior evidence indicates that the PL/ILA and PVT regions play a role in regulating sleep and arousal in both cortical and subcortical areas [20]. The SLD has been reported to stabilize REM sleep, while dopaminergic neurons in the DR are involved in sleep-wake regulation [21, 22]. (2) Pain modulation, KET significantly activated pain-related areas such as the anterior cingulate cortex (ACA) in the cortex [23], the anterior pretectal nucleus (APN) in the thalamus, which is known to be involved in managing chronic pain [24], and the anterior periaqueductal gray (PAG) region and medial prefrontal cortex (mPFC), both part of the endogenous pain inhibitory pathway [25, 26],. Additionally, the activation of the locus coeruleus (LC) in the midbrain may contribute to KET's analgesic effects [27]. (3) Neuroendocrine regulation: The paraventricular hypothalamic nucleus (PVH) and supraoptic nucleus (SON), which are neuroendocrine-related regions, were also activated [18, 28]. (4) Movement: Subcortical nuclei associated with movement, such as the subthalamic nucleus (STN) and nucleus incertus (NI), were prominently activated by KET administration [29, 30]. (5) Connectivity: We observed significant activation of the nucleus reunions (Re) located in the thalamus, which receives substantial afferent input from limbic structures and serves as a connector linking the hippocampus to the medial prefrontal cortex [31]. In summary, our study identified extensive activation of cortical and subcortical nuclei during KET anesthesia, encompassing regions related to arousal, pain modulation, neuroendocrine regulation, movement, and connectivity.

Identifying brain regions activated by ISO

In our study, we aimed to identify brain regions activated by ISO and compare these with those activated by KET. We began by summarizing previously reported ISO activated nuclei, including PIR, LSd/LSv, CeA in the cortex and striatum, and VLPO, MnPO, EW, NTS, LC, ventral group of the dorsal thalamus (VeN), and area postrema (AP) in the hypothalamus and midbrain (Supplementary Table 3). We subsequently conducted a comprehensive MATLAB-based analysis of c-Fos expression throughout the entire brain, uncovering previously undetected activated nuclei (Figure 5A, Supplementary Figure 2). Newly identified activated nuclei in the CTX and the CNU included PL/ILA and ENT, aPVT in the thalamus, TU, ARH, PVi, and PVH in the hypothalamus, and PB in the hindbrain. All nuclei activated by ISO in this study were functionally classified and depicted in Figure 5C. Our results confirmed the activation of several brain regions involved in sleep-wakefulness regulation, such as the prelimbic area (PL) and infralimbic areas (ILA), and the anterior paraventricular nucleus (aPVT), leads to increased NREM sleep and decreased wakefulness [20]. Additionally, we observed activation in previously reported analgesia-related nuclei, including CeA and LC, as well as the parabrachial nucleus (PB) [18, 27, 32]. We also found activation in neuroendocrine function-related nuclei of the hypothalamus, such as TU, PVi, ARH, PVH, and SON. Moreover, we identified activations related to ISO induced side effects, such as in the piriform cortex (PIR) [33] and ENT [34]. which may be stimulated by ISO odor, and the solitary tract nucleus (NTS), potentially responsible for ISO induced vomiting [35]. The only activated nucleus in the midbrain was the Edinger-Westphal nucleus (EW). Recent research has found that sevoflurane activates EW and is involved in sleep induction and maintenance of anesthesia, suggesting its crucial role in general anesthesia [36]. By comparing the ISO and KET induced c-Fos expression, we summarized the brain regions activated by both anesthetics in Figure 5D. Despite variations in molecular targets, the coactivation of regions such as PL/ILA, aPVT, CeA, PVH, SON, EW, PB, LC, and NTS by both ISO and KET suggests an overlapping neuronal circuitry that influences sleep-wake regulation, analgesia, and neuroendocrine functions. This shared neural circuitry may po-

tentially offer a common mechanism across the two anesthetics for the maintenance of general anesthesia.

Network generation and Hub identification

Previous research has established that general anesthesia is mediated by various brain regions [7, 16-18]. c-Fos expression serves as an indicator of neuronal activity, providing a single index of activation per region per animal. By examining the covariance of c-Fos expression across animals within each group, we can infer interactions between brain regions and identify functional networks engaged during general anesthesia [37]. Highly correlated activities across different brain regions are presumed to constitute components of a functional network, reflecting the complex interplay of brain areas during general anesthesia. We first employed c-Fos expression as a neuronal activity marker and calculated a comprehensive set of interregional correlations for four groups. The matrices exhibited interregional correlations for the number of c-Fos-positive cells in each condition (Figure 6A). Network graphs were generated by extracting Pearson's coefficients > 0.82, as well as significant positive correlations ($P < 0.05$), from these matrices to construct functional brain networks (Figure 6B). In comparison to the control group, isoflurane (ISO) slightly decreased interconnections between regions (network density: 0.13 vs. 0.10; edges: 267 vs. 198), with no significant difference in mean interregional correlation coefficients between the ISO group and the home cage group (Fisher $Z = -0.018$, $P = 0.98$). Conversely, ketamine (KET) significantly increased the network's connectivity density (network density: 0.13 vs. 0.47; edges: 265 vs. 1008) and showed a significant increase in mean interregional correlation coefficients compared to the saline group (Fisher $Z = 3.54$, $P < 0.001$) (Figure 6C). These findings suggest that ISO may exert a mild inhibitory effect on functional network connectivity, whereas KET appears to enhance interregional correlation following administration (Figure 6D).

Hubs are nodes that occupy critical central positions within the network, enabling the network to function properly. To determine the brain regions that serve as the hubs for ISO and KET induced functional networks, we calculated each node's degree (the number of links that connect it) and betweenness centrality (the fraction of all shortest paths in the network that contain a given node). Nodes with a high degree and betweenness centrality typically have a

lot of connections. We ranked each node according to its degree and betweenness centrality and extracted nodes with a rank greater than the 80th percentile in its network. Additionally, we segmented the functional network into non-overlapping modules using a spectral community detection algorithm and calculated the within-modal degree Z-score (the degree of nodes within a module, which indicates within-module connectivity) as well as participation coefficients (the distribution of the edges of a node between other modules, which indicates within-module connectivity) [38]. Nodes with relatively high values for both parameters were considered relatively significant within and outside the network module. We classified nodes with participation coefficients > 0.4 and Z scores > 1 as connector hubs [39]. The LC, exhibiting elevated degree and betweenness centrality as well as relatively higher Z-scores and participation coefficients, may play a pivotal role in mediating isoflurane-induced general anesthesia, given its known involvement in arousal, attention, and analgesia. In contrast, the somatosensory cortex (SS) functions as a connector hub in the KET group, indicating its integrative and coordinating role in ketamine-induced dissociative anesthesia (Figure 7D). The LSc served as the central hub in the saline group (Figure 7C). No significant findings were observed in the within-modal degree Z-score and participation coefficient analyses for the home cage group. However, the analysis did reveal a relatively high degree and betweenness centrality of APNs (Figure 7A), suggesting that the within-module connections are relatively independent, or that the pathways of inter-module information transmission do not depend on specific connector nodes.

Discussion

In this study, we conducted a comparative analysis of the effects of two general anesthetics, isoflurane (ISO) and ketamine (KET), on c-Fos expression throughout the brain. By employing principal component analysis (PCA), we were able to thoroughly examine the responses of individual brain regions to each anesthetic agent. Our findings reveal that KET dominantly activates the cerebral cortex yet suppresses subcortical regions, reflecting a top down mechanism of action, while ISO predominantly stimulates subcortical brain regions with relative cortical inhibition, substantiating its bottom up mechanism of action [3, 4]. Further functional analysis of brain networks, based on c-

Fos expression, identified the somatosensory cortex (SS) and the locus coeruleus (LC) as central nodes for KET and ISO, respectively, highlighting the crucial roles of LC and SS under ISO and KET induced unconsciousness.

Our results demonstrate that ISO activates the sleep-promoting VLPO nucleus, the aPVT-infralimbic loop [20], and broadly inhibits the cortex, supporting a bottom-up mechanism of ISO induced unconsciousness. Nonetheless, our findings also reveal the activation of arousal related nuclei, such as PB and LC, which implies that the influence of isoflurane on consciousness may not solely rely on suppressing arousal centers, but rather through a more intricate relationship than formerly recognized. Identifying cell types and their dynamic changes during anesthesia will be crucial for clarifying their role in ISO induced unconsciousness.

While c-Fos-based functional network analysis offers lower temporal resolution, its single-cell resolution across the entire brain allows for the inclusion of midbrain and hindbrain regions, supplementing previous fMRI analyses. Our observations reveal that ISO mildly inhibits network density, and through graph theoretical analysis, we identify the LC as a highly connected hub, highlighting the critical role of the brainstem in ISO induced general anesthesia. The LC performs a wide range of functions in mice, including arousal, pain modulation, attention, stress response, and neuroprotection. Studies have shown that chemical activation of the LC increases whole-brain functional connectivity, attributed to its role as the primary source of norepinephrine (NE) and its extensive influence on nearly the entire brain [40]. The significant LC activation and its central position within the functional network underlying ISO induced unconsciousness suggest that the LC plays a crucial part in maintaining and integrating the entire unconsciousness functional network, emphasizing the involvement of LC in the bottom-up paradigm of ISO induced unconsciousness.

Mashour et al. proposed that anesthesia-induced unconsciousness encompasses not only the modulation of lower-level brain activity but also top down neural processing [3, 4]. Within this top down framework, anesthetics diminish consciousness by interfering with cortical and thalamocortical circuits responsible for neural information integration. Our study discovered that KET administration substantially activated cortical and subcortical arousal-

promoting nuclei while concurrently causing relative thalamic suppression, with only the RE and TRS exhibiting activation. This suggests that thalamic inhibition may lead to a reduction in thalamocortical communication, which is characterized by the inability to perceive the external environment and results in disconnection from reality. Graph theoretical analysis also identified the somatosensory cortex (SS) as the hub node of the KET induced functional network. As a critical cortical area, SS is responsible for sensory processing, motor control, and cognitive functions [41]. Previous studies have demonstrated that local KET administration to SS recapitulates the effects of systemic KET on both the switch in pyramidal cell activity and dissociative-like behavior, implying that SS may serve as a key target for KET induced dissociation [42]. Our findings that SS acts as a hub node suggest that KET may modulate brain network function by influencing connectivity between SS and other brain regions, thereby affecting the behavior and cognitive states of mice. This further supports the significance of cortical areas during KET anesthesia.

Identifying shared neural features between KET and ISO is essential for understanding anesthetic-induced unconsciousness. The coactivation of sleep-wake regulation-related regions, such as PL/ILA and aPVT, along with analgesia-related nuclei like CeA, PB, and LC, suggests a shared mechanism for sleep-wake regulation and the common pathways for pain relief. This observation provides valuable insights into the fundamental mechanisms of anesthesia-induced hypnosis and analgesia. Additionally, the coactivation of neuroendocrine-related nuclei, including PVH and SO in the hypothalamus, raises questions about the potential influence of anesthetics on hormonal release and homeostatic regulation. Other coactivated nuclei, such as EW and NTS, warrant further investigation of their roles in anesthesia. In summary, the coactivated nuclei imply a potential shared neuronal circuitry for general anesthesia, encompassing common features like unconsciousness, analgesia, and autonomic regulation, regardless of the specific molecular targets of each drug. Future research could examine coactivated brain regions by the two anesthetics or manipulate identified hub nodes to further understand the mechanisms of general anesthesia. In summary, our study reveals distinct and shared neural mechanisms underlying isoflurane and ketamine anesthesia

using c-Fos staining and network analysis. Our findings support "top-down" and "bottom-up" paradigms, and the identification of hub nodes and coactivated brain regions suggests shared neurocircuitry for general anesthesia, providing insights into the mechanisms underlying anesthetic-induced unconsciousness and analgesia.

Methods

Animals

All animal experiments were conducted in accordance with the National Institutes of Health guidelines and were approved by the Chinese Academy of Sciences' Institute of Neuroscience. Adult male wild-type (WT) mice (C57BL/6J) (8-10 weeks old, weight from 22 to 26 g) were purchased from institute-approved vendors (LingChang Experiment Animal Co., China). Mice were individually housed and maintained on a 12 h:12 h light/dark cycle (lights on at 07:00 a.m. and off at 07:00 p.m.) with food and water available ad libitum.

Drug administration

All experiments occurred between 13:00-14:30 (ZT6–ZT7.5). We adapted mice to handling and the anesthesia chamber (10×15×15 cm) for several days to minimize experimental confound-induced c-Fos induction. Adult male mice were handled for the KET group for 10 min per day with normal saline (NS) injected intraperitoneally (i.p.) for three consecutive days at 13:00. On day five, a randomly chosen mouse received an injection of Ketamine (Gutian Medicine, H35020148), and the control groups (n=8) received the same volume of saline. ISO group (n=6) mice were handled and inhaled 1.5% isoflurane (RWD Life Science, 1903715) at 13:00 on day four in the chamber. Meanwhile, the control groups (n=6) were left undisturbed in their home cages prior to sampling. We confirmed the loss of righting reflex at 5 min after anesthetics exposure. For 90 min after KET injection or ISO inhalation, mice were deeply anesthetized with 5% ISO and transcardially perfused with 35ml 0.1 M phosphate-buffered saline (PBS) followed by 35ml 4% paraformaldehyde (PFA). The brains were then removed and postfixed overnight with 4% PFA. Following fixation, the brains were dehydrated for 48 hours with 30% sucrose (wt/vol) in PBS. Coronal sections (50 μm) of the whole brain were cut using a cryostat

(HM525 NX, Thermo Scientific) after being embedded with OCT compound (NEG-50, Thermo Scientific) and freezing.

Immunohistochemistry

One out of every three brain slices (100 μm intervals) of each whole brain was washed three times with 0.1 M phosphate-buffered saline (PBS) for 10 min and permeabilized for 30 minutes at room temperature with 0.3% Triton X-100 in PBS (PBST). Slices were incubated for 2 hours at room temperature with 2% normal donkey serum (Sigma, G6767) in PBS overnight at 4°C with c-Fos primary antibodies (226003, Synaptic Systems; 1:500) diluted in PBS with 1% donkey serum. After three washes with PBST, slices were incubated with the Cy3 donkey anti-rabbit (711165152, Jackson; 1:200) secondary antibody for 2 hours at room temperature. Immunostained slices were mounted with VECTASHIELD mounting medium with DAPI and then scanned under a fluorescent microscope equipped with a 10× objective (VS120, Olympus) or a confocal microscope with a 20× objective (FV300, Olympus).

Quantification of c-Fos positive cells

The procedures used for c-Fos analysis were based on previously research [19]. A custom-written software package was employed for the analysis of brain images. The software consists of four modules: atlas rotation, image registration, signal detection, and quantification/visualization.

Rotation module

The rotation module allows the Allen Mouse Brain Atlas to be rotated in three dimensions at arbitrary angles to fit individual samples. Anatomical landmarks were manually selected to estimate rotation angles. The most posterior slices containing the CA3 in each hemisphere were used to calculate the rotation angle about the left-right axis. The most anterior slice with the anterior commissure crossing the midline and the most posterior slice with the corpus callosum crossing the midline were used to calculate the rotation angle about the dorsal-ventral axis. The reference atlas was then rotated using these estimated angles to match the experimental brain's sectioning angle.

Registration module

The registration module is an image alignment software that uses reference points to align brain section images with a rotated 3D reference atlas for further quantification. First, reference points in both the atlas and the brain

image were chosen. The module then applied geometric transformations to the brain section to optimize the match between the brain image and the atlas's reference points. After the transformation, the image was compared to the atlas, and any necessary adjustments were made manually.

Detection module

The detection module manually counts the position of c-Fos positive cells in each digitized brain section image.

Principal components analysis (PCA) of the activity patterns at whole brain

We employed arithmetic to calculate the cell density in each brain region:

$$x_R = \log 10 \left[\frac{(N_r + 1)}{V_r} \Big/ \frac{\sum_1^R (N_r + 1)}{\sum_1^R V_r} \right]$$

Nr: The number of c-Fos+ cells in each brain region. Vr: The volume of each brain region. The density of c-Fos from 201 brain regions were concatenated for each mouse (Home cage, n = 6; ISO, n = 6; Saline, n = 8; KET, n = 6). Principal components analysis was performed on the concatenated matrix containing data from four conditions, using singular value decomposition. We then selected the first two principal components (PCs), which accounted for 56.6% of the variance in Figure 2A and 44.5% in Figure 3A.

Network generation

To evaluate how functional connectivity changed under general anesthetics in WT mice, we extracted 63 brain regions from major brain subdivisions (cerebral cortex, cerebral nuclei, thalamus, hypothalamus, midbrain, and hindbrain) listed in Supplementary Table 2. Correlation matrices were generated by computing Pearson correlation coefficients from interregional c-Fos expression in the 63 regions. Mean correlations were calculated to assess changes in functional connectivity between these major subdivisions of the brain. Weighted undirected networks were constructed by considering correlations with Pearson's r ≥0.82, corresponding to a one-tailed significance level of P<0.05 (uncorrected). The nodes in the networks represent brain regions, and the correlations that survived thresholding were considered connections. Theoretical graph analysis was performed using Brain Connectivity Toolbox

(https://sites.google.com/site/bctnet/, version 2019-03-03) in MATLAB R2021 (The MathWorks Inc.) [43]. Network visualization was performed using Cytoscape (version 3.2.1) [44].

Hub identification

Network centrality was evaluated using degree, betweenness, within-module z-scores (representing within-module connectivity), and participation coefficient (indicating between-module connectivity). These measures were computed for all nodes to identify potential hub regions [45]. Modularity was assessed employing Newman's spectral community detection algorithm [46]. Degree represents the number of edges connected to a node, while betweenness denotes the number of shortest paths traversing a given node. Nodes with elevated betweenness centrality are involved in numerous shortest paths.

Statistical analysis

The sample size was determined based on prior studies [13, 14]. Normality of data distribution was assessed using the Shapiro-Wilk W test. Unpaired Student's t-test was applied for normally distributed data, while the Mann-Whitney U test was employed for non-normally distributed data. Data are presented as mean ± SEM, with all statistical tests being two-sided. Pearson correlation coefficients (R) were transformed into Z-scores using Fisher's Z transformation before computing group means and conducting statistical comparisons. GraphPad Prism 9.0 (GraphPad Software, USA) and MATLAB R2021 (Mathworks Inc.) were utilized for statistical analyses. A P-value less than 0.05 was considered statistically significant.

Acknowledgements

We express our gratitude to our interns, Chuhang Wong from Imperial College London and Jiale Huang from ShanghaiTech University, for their assistance in cell counting.

Funding

This study was funded by the NSFC (grants 82271292, 81730031 to Y.W.; 82101350 to M.L.) and the Shanghai Municipal Key Clinical Specialty (grant shslczdzk06901 to Y.W.).

Author contributions

Yue Hu, Conceptualization, Formal analysis, Investigation, Visualization, Methodology, Writing—original draft, Writing—review and editing; Jiangtao Qi, Conceptualization, Software, Formal analysis, Investigation, Methodology, Writing—original draft, Writing—review and editing; Zhao Zhang, Resources, Investigation, Supervision, Writing—review and editing; Mengqiang Luo, Resources, Supervision, Funding acquisition, Project administration, Writing—review and editing; Yingwei Wang, Conceptualization, Resources, Supervision, Funding acquisition, Project administration, Writing—review and editing.

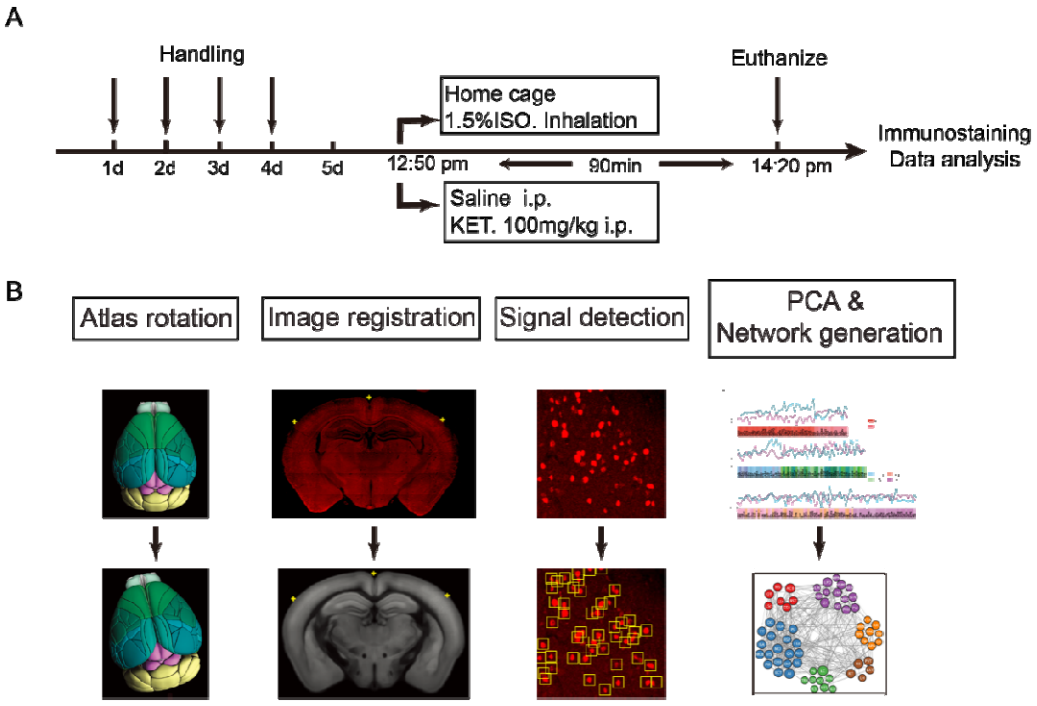

Figure 1. Brain-wide quantification of c-Fos expression.

(A) Schematic representation of the habituation protocol typically used to acclimate mice. After being exposed to anesthetics for 90 minutes, the mice were euthanized. (B) Steps for data processing. Example of brain section registration to a corresponding coronal section from the Allen Brain Atlas. For Atlas rotation, the Allen reference atlas was rotated to mimic the slice

angle of the experimental brain. Image registration maps the original coronal image (upper panel) to the corresponding Allen mouse brain atlas (lower panel). The registration module applies several geometric transformations (translation, rotation, and scaling) to optimize the matching of the original image to the anatomical structures. Fluorescence signals were detected from the original image (upper panel), and once detected, they were projected onto the Allen Mouse Brain Atlas for quantification and network analysis by means of the detected signals labeled with yellow boxes.

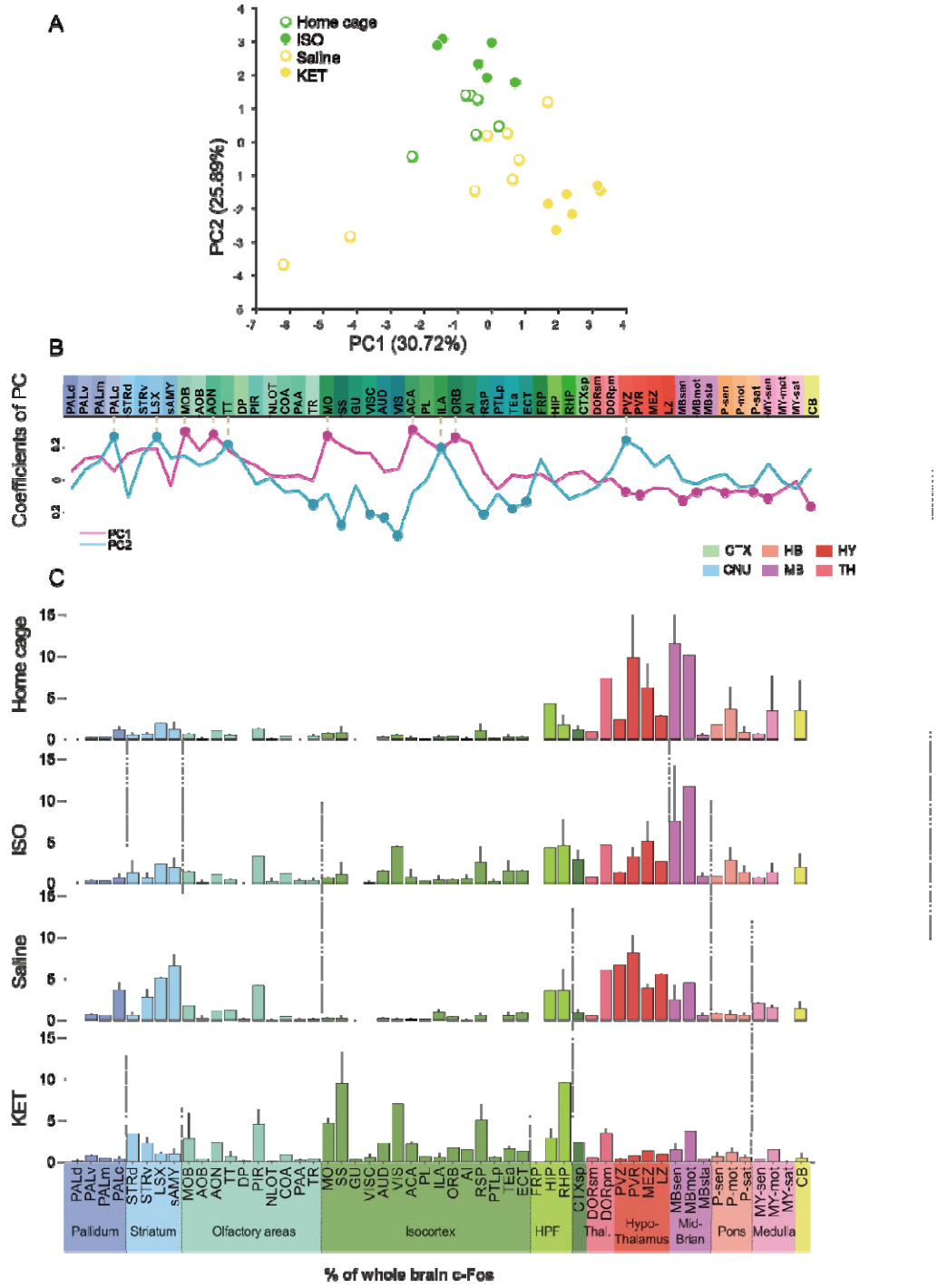

Figure 2. Whole-brain distributions of c-Fos$^+$ cells induced by ISO, KET, and control conditions. (A) Scatter plot of four conditions in the space spanned by the first two principal components (PC1 versus PC2) of c-Fos density from 53 brain regions. (B) Line plot of coefficients of PC1 and PC2. Dots represent regions with absolute values larger than 75 percentiles. (C)

The normalized c-Fos$^+$ cells in 53 brain areas (Home cage, n = 6; ISO, n= 6 mice; Saline, n = 8; KET, n = 6). Brain areas are grouped into 12 generalized, color-coded brain structures. Abbreviations of the 53 brain areas and percentages of c-Fos+ cells are listed in supplementary table 1. Error bar, mean ± SEM.

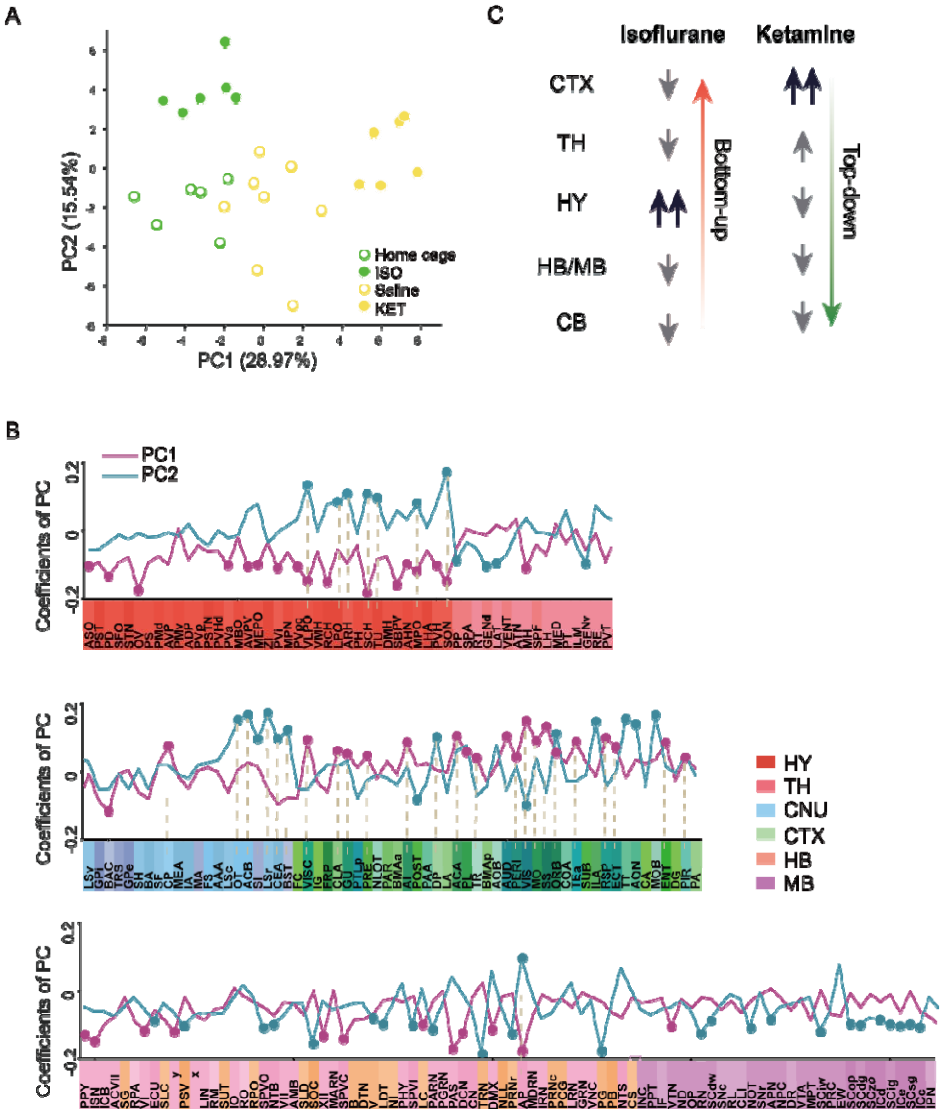

Figure 3. Similarities and differences in ISO and KET activated c-Fos brain areas. (A) Scatter plot of four conditions in the space spanned by the first two principal components (PC1 versus PC2) of normalized c-Fos density from 201 brain regions. (B) Line plot of coefficients of PC1 and PC2. Dots rep-

resent regions with absolute values larger than 75 percentiles. (C) Activation patterns of ISO and KET in different parts of brain regions were summarized. ISO was predominantly characterized by increased activation of hypothalamic and cerebral nuclei while reducing activity in the cortex and midbrain, indicating that ISO primarily exerts its effects through a bottom-up mechanism. On the other hand, KET primarily activated the cortex and inhibited hypothalamus and midbrain activity, suggesting that KET regulates consciousness through a top-down mechanism.

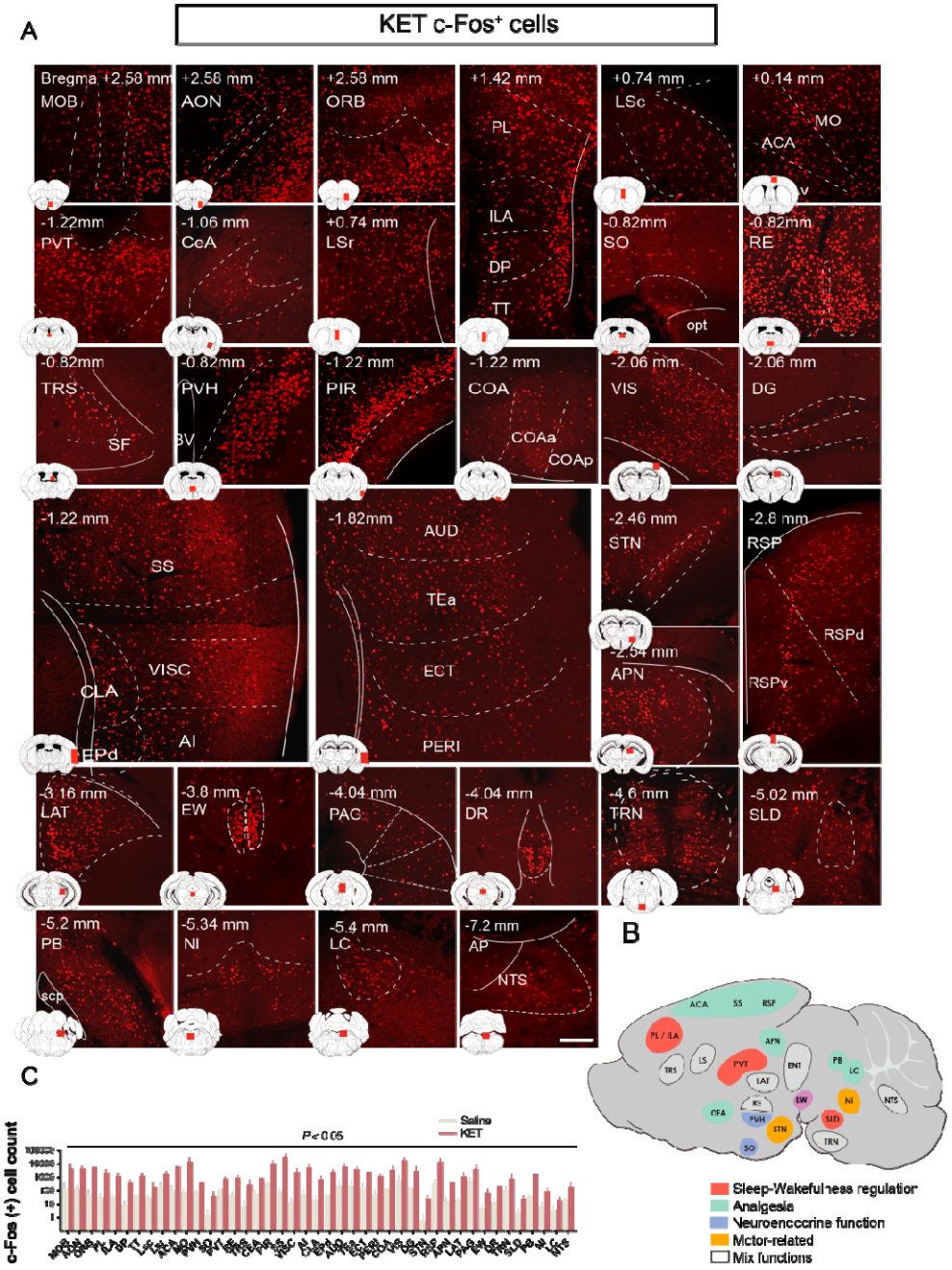

Figure 4. c-Fos expression in distinct brain regions after exposure to KET. (A) Representative immunohistochemical staining of MOB, AON, ORB, MPO, ACA, MO, TRS, PL, ILA, DP, LS, PVT, SO, PVH, RE, VISC, AI, CLA, EPd, PIR, COA, AUD, TEa, ECT, PERI, CeA, SS, DG, STN, RSP, APN, LAT, EW, DR, PAG, SLD, PB, TRN, NI, LC, NTS, and NI c-Fos^{+} cells from the indicated mice. Scale bar, 200 μm. (B) Cell counts of saline group and KET group compared with *P* values < 0.05. Data are represented as mean ± SEM. (C)

Schematic cross-section of the mouse brain showing activated brain regions by KET. Different colors indicate distinct functional nuclei. The red nuclei are associated with the regulation of sleep-wakefulness, the blue-green nuclei are linked to analgesia, the yellow nuclei are associated with motor function, and the white nuclei are a composite of various functional nuclei.

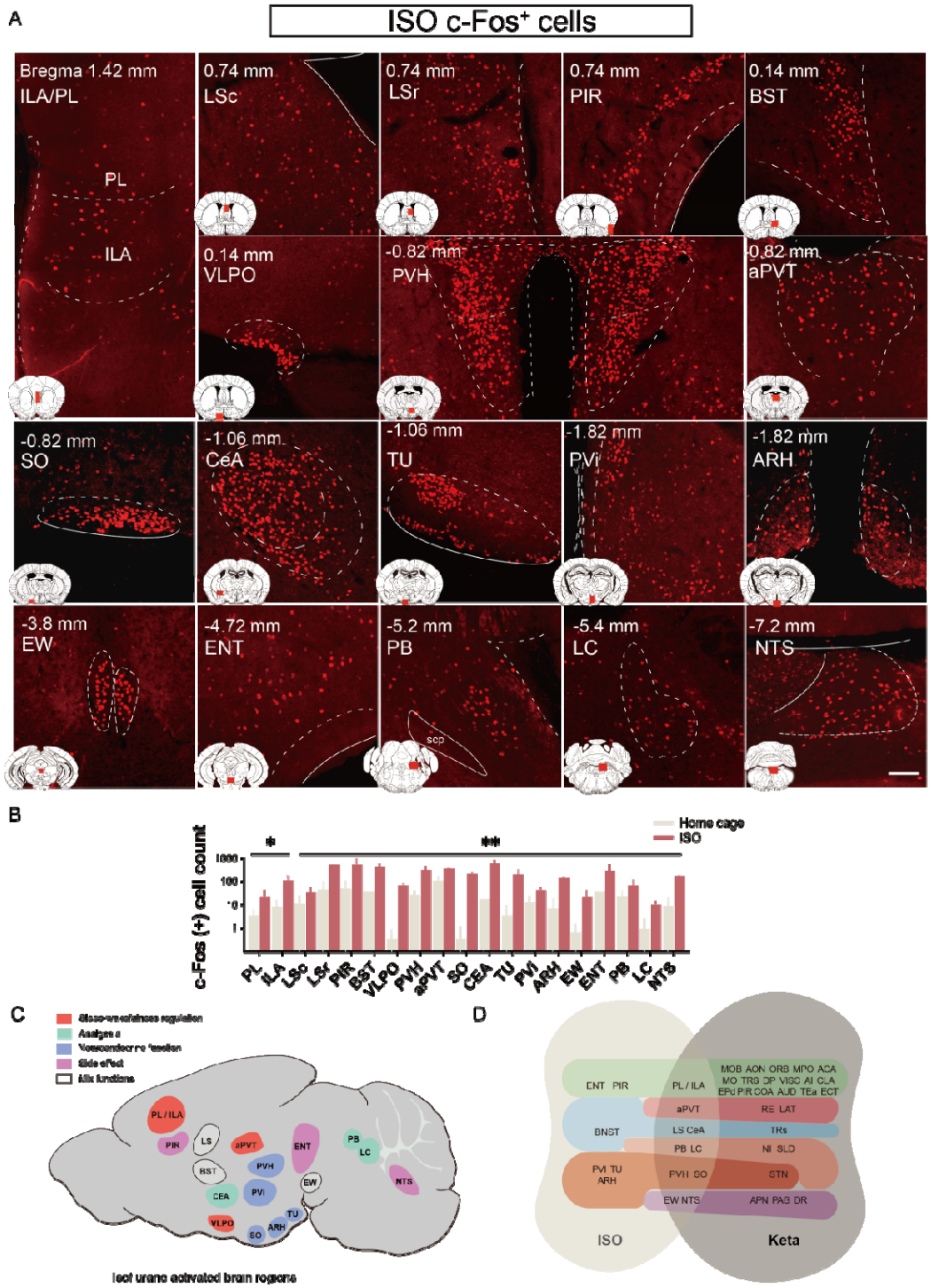

Figure 5. c-Fos expression in distinct brain regions after exposure to ISO. (A) Representative of brain regions with statistical differences c-Fos$^+$ cells between the ISO group and home cage mice. Scale bar, 200 μm. (B) Cell counts of home cage group and ISO group compared with T-test, *P* values < 0.05. Data are represented as mean ± SEM (C) Schematic cross-

section of the mouse brain showing activated brain regions by ISO. Different colors indicate various functionally relevant nuclei. Red signifies nuclei involved in sleep-wake regulation, blue-green in pain management, blue in neuroendocrine function, pink in side-effect management, and white denotes nuclei exhibiting mixed functionalities. (D) The Venn diagram shows brain regions that are co-activated by ISO and KET and differentially activated brain regions(Manual calibration and T-test correction).

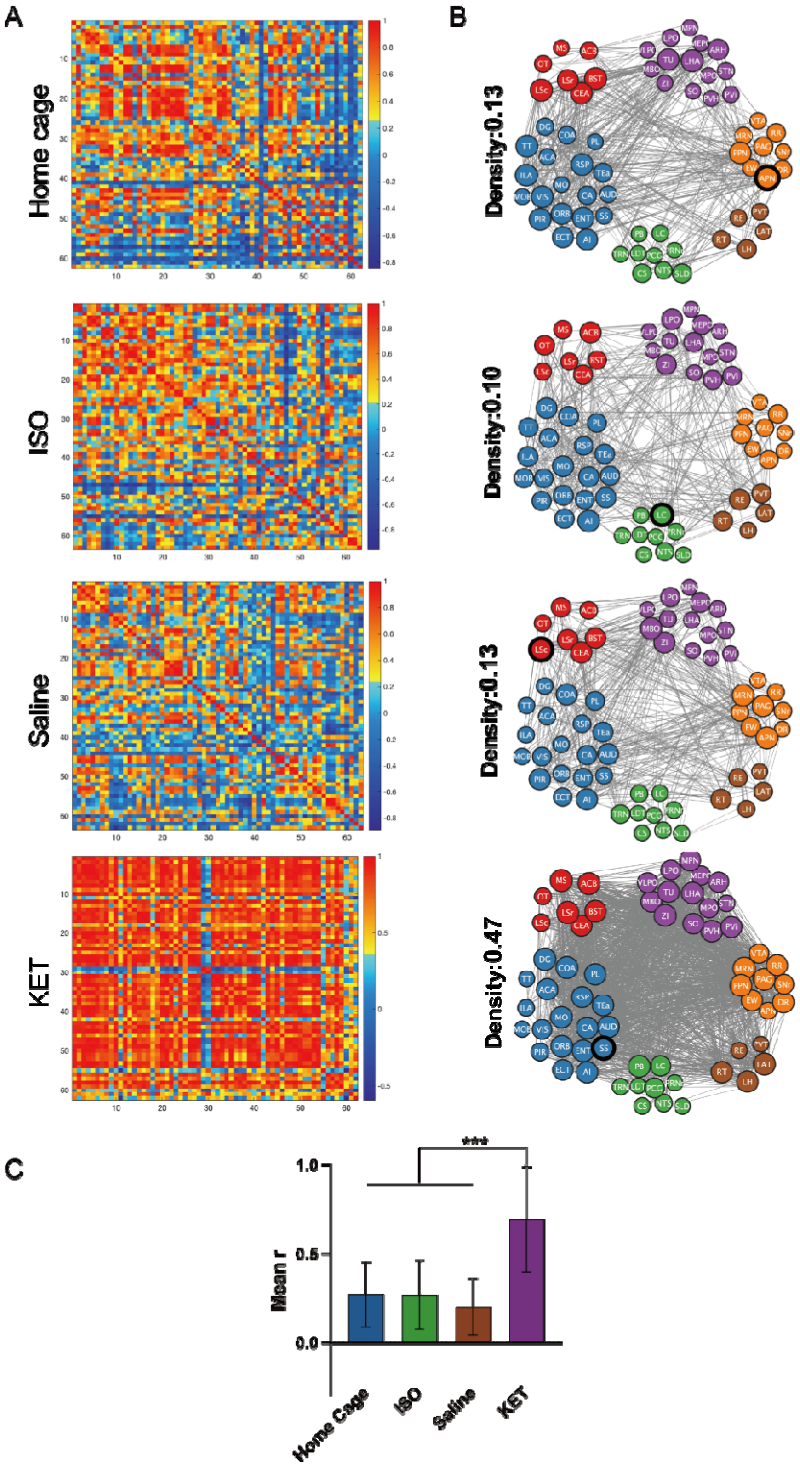

Figure 6. Generation of anesthetics-induced networks and identification of hub regions. (A) Matrices showing interregional correlations for c-Fos expression at the home cage, ISO, saline, and KET. Colors reflect correlation strength based on Pearson's r (color bar, right). Axes are numbered and cor-

respond to brain regions listed in Supplementary Table 5. (B) Network graphs were generated by significant positive correlations ($P < 0.05$), as well as Pearson's $r > 0.82$. The widths of the edges are proportional to the strength of the correlations and the size of the nodes is proportional to the degree of the node. Colors represent the major brain division (red, cerebral nuclei; purple, hypothalamus; orange, midbrain; brown, thalamus; blue, thalamus; green, the cerebral cortex. Network densities were noted in the left. (C) Mean r was calculated from interregional correlation coefficients.

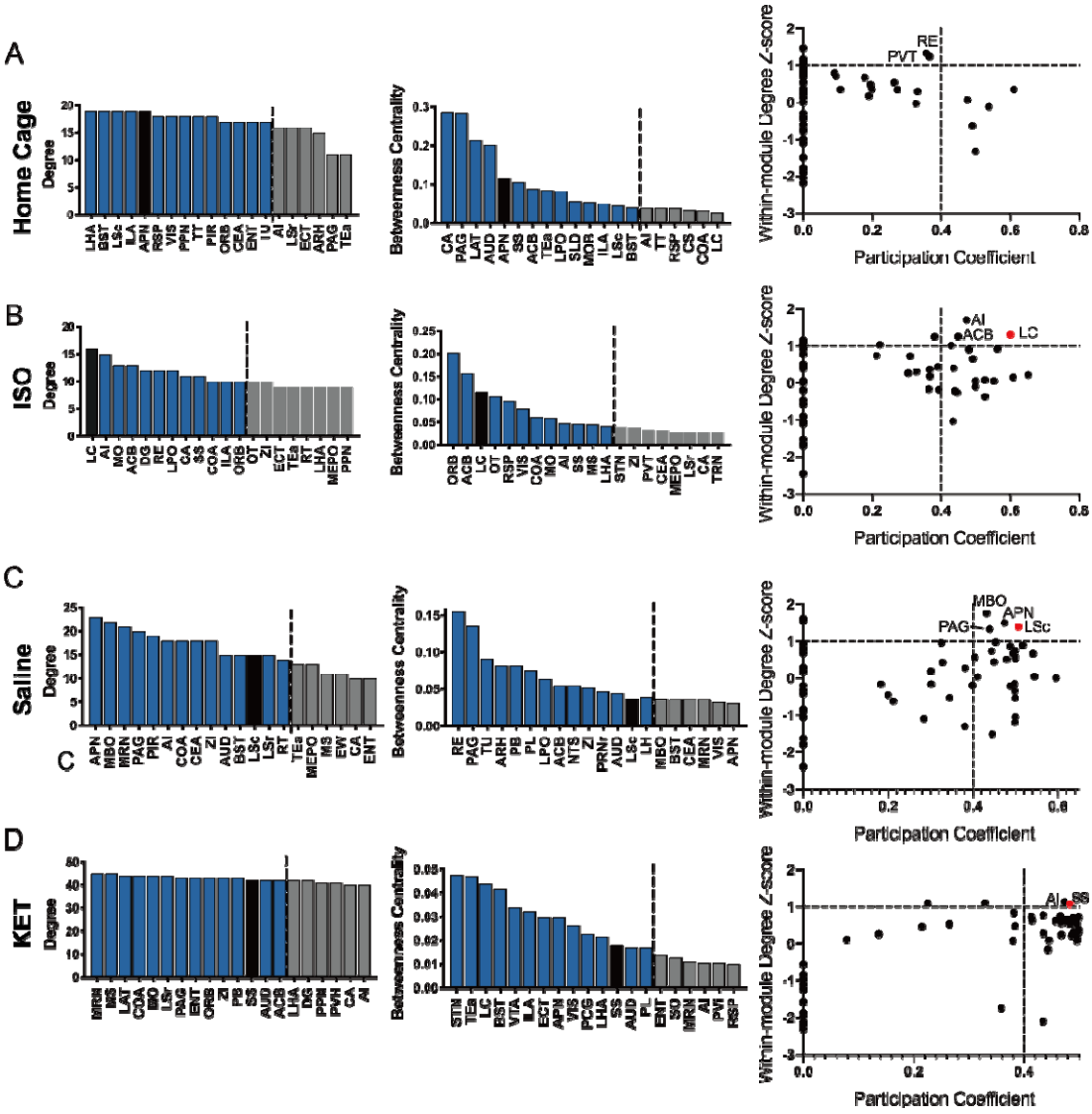

Figure 7. Identification of hub regions in the home cage (A), ISO (B), NS (C), and KET (D) groups. The degree and betweenness centrality for each brain region are ranked in descending order. Black columns indicate the overlap of brain regions that rank within the top 20% for both degree and betweenness centrality. The dotted line signifies the ranking threshold, encompassing greater than 80% of the brain regions in our network. The within-community Z-scores and participation coefficients are calculated for each brain region in the networks. Brain regions with a participation coefficient greater than 0.4 and a within-module degree Z-score greater than 1 are defined as hubs, as represented by the red dots.

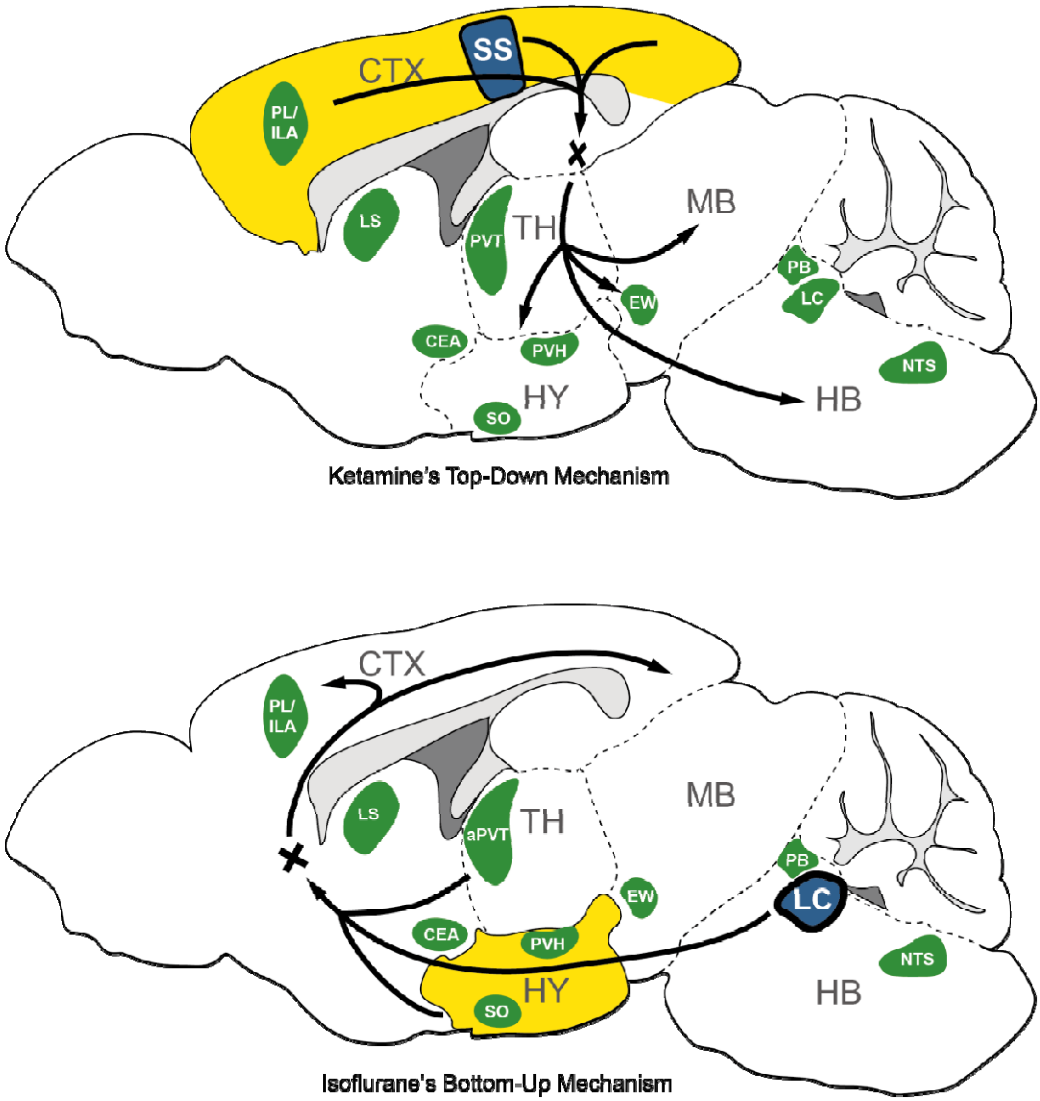

Figure 8. The possible framework for ketamine and isoflurane induced unconsciousness. The distinct pathways of ketamine and isoflurane induced unconsciousness can be explained by two contrasting mechanisms. The "top-down" process attributes KET's effect to widespread cortical activation (represented in yellow), with the somatosensory cortex (SS) acting as the central node in the functional network (depicted in blue) and relative inhibition of hypothalamic sleep-promoting nuclei. Conversely, the "bottom-up" approach posits that isoflurane induced unconsciousness arises from the activation of hypothalamic sleep-promoting regions (indicated in yellow) and relative inhibition of cortical and thalamic nuclei, with the locus coeruleus (LC) serving as the hub node in the isoflurane induced functional network. Nuclei activated by both anesthetics are shown in green. Adapted from [3, 4, 47]. PL, prelimbic area; ILA, infralimbic areas; SON, supraoptic nucleus; PVH, paraventricular hypothalamic nucleus; TU, tuberal nucleus; LC, locus coeruleus; SS, somatosensory cortex; CTX: cortex; TH: thalamus; HY, hypothalamus; MB; midbrain; HB, hindbrain.

References

1. Hemmings HC, Jr., Riegelhaupt PM, Kelz MB, Solt K, Eckenhoff RG, Orser BA, Goldstein PA: **Towards a Comprehensive Understanding of Anesthetic Mechanisms of Action: A Decade of Discovery**. *Trends Pharmacol Sci* 2019, **40**(7):464-481.
2. Franks NP: **General anaesthesia: from molecular targets to neuronal pathways of sleep and arousal**. *Nat Rev Neurosci* 2008, **9**(5):370-386.
3. Mashour GA: **Top-down mechanisms of anesthetic-induced unconsciousness**. *Front Syst Neurosci* 2014, **8**:115.
4. Mashour GA, Hudetz AG: **Bottom-Up and Top-Down Mechanisms of General Anesthetics Modulate Different Dimensions of Consciousness**. *Front Neural Circuits* 2017, **11**:44.
5. Schroeder KE, Irwin ZT, Gaidica M, Nicole Bentley J, Patil PG, Mashour GA, Chestek CA: **Disruption of corticocortical information transfer during ketamine anesthesia in the primate brain**. *NeuroImage* 2016, **134**:459-465.
6. Lee U, Ku S, Noh G, Baek S, Choi B, Mashour GA: **Disruption of frontal-parietal communication by ketamine, propofol, and sevoflurane**. *Anesthesiology* 2013, **118**(6):1264-1275.
7. Moore JT, Chen J, Han B, Meng QC, Veasey SC, Beck SG, Kelz MB: **Direct Activation of Sleep-Promoting VLPO Neurons by Volatile Anesthetics Contributes to Anesthetic Hypnosis**. *Curr Biol* 2012, **22**(21):2008-2016.
8. Nelson LE, Guo TZ, Lu J, Saper CB, Franks NP, Maze M: **The sedative component of anesthesia is mediated by GABA(A) receptors in an endogenous sleep pathway**. *Nat Neurosci* 2002, **5**(10):979-984.
9. Yap EL, Greenberg ME: **Activity-Regulated Transcription: Bridging the Gap between Neural**

Activity and Behavior. *Neuron* 2018, **100**(2):330-348.

10. Morgan JI, Curran T: **Stimulus-transcription coupling in neurons: role of cellular immediate-early genes**. *Trends Neurosci* 1989, **12**(11):459-462.
11. Zhang D, Liu J, Zhu T, Zhou C: **Identifying c-fos Expression as a Strategy to Investigate the Actions of General Anesthetics on the Central Nervous System**. *Curr Neuropharmacol* 2022, **20**(1):55-71.
12. Smith ML, Li J, Cote DM, Ryabinin AE: **Effects of isoflurane and ethanol administration on c-Fos immunoreactivity in mice**. *Neuroscience* 2016, **316**:337-343.
13. Lu J, Nelson LE, Franks N, Maze M, Chamberlin NL, Saper CB: **Role of endogenous sleep-wake and analgesic systems in anesthesia**. *J Comp Neurol* 2008, **508**(4):648-662.
14. Yatziv SL, Yudco O, Dickmann S, Devor M: **Patterns of neural activity in the mouse brain: Wakefulness vs. General anesthesia**. *Neurosci Lett* 2020, **735**:135212.
15. Han B, McCarren HS, O'Neill D, Kelz MB: **Distinctive recruitment of endogenous sleep-promoting neurons by volatile anesthetics and a nonimmobilizer**. *Anesthesiology* 2014, **121**(5):999-1009.
16. Gelegen C, Miracca G, Ran MZ, Harding EC, Ye Z, Yu X, Tossell K, Houston CM, Yustos R, Hawkins ED *et al*: **Excitatory Pathways from the Lateral Habenula Enable Propofol-Induced Sedation**. *Curr Biol* 2018, **28**(4):580-587.e585.
17. Hua T, Chen B, Lu D, Sakurai K, Zhao S, Han BX, Kim J, Yin L, Chen Y, Lu J *et al*: **General anesthetics activate a potent central pain-suppression circuit in the amygdala**. *Nat Neurosci* 2020, **23**(7):854-868.
18. Jiang-Xie LF, Yin L, Zhao S, Prevosto V, Han BX, Dzirasa K, Wang F: **A Common Neuroendocrine Substrate for Diverse General Anesthetics and Sleep**. *Neuron* 2019, **102**(5):1053-1065.e1054.
19. Ma G, Liu Y, Wang L, Xiao Z, Song K, Wang Y, Peng W, Liu X, Wang Z, Jin S: **Hierarchy in sensory processing reflected by innervation balance on cortical interneurons**. *Science Advances* 2021, **7**(20):eabf5676.
20. Gao C, Leng Y, Ma J, Rooke V, Rodriguez-Gonzalez S, Ramakrishnan C, Deisseroth K, Penzo MA: **Two genetically, anatomically and functionally distinct cell types segregate across anteroposterior axis of paraventricular thalamus**. *Nat Neurosci* 2020, **23**(2):217-228.
21. Feng H, Wen SY, Qiao QC, Pang YJ, Wang SY, Li HY, Cai J, Zhang KX, Chen J, Hu ZA *et al*: **Orexin signaling modulates synchronized excitation in the sublaterodorsal tegmental nucleus to stabilize REM sleep**. *Nat Commun* 2020, **11**(1):3661.
22. Cho JR, Treweek JB, Robinson JE, Xiao C, Bremner LR, Greenbaum A, Gradinaru V: **Dorsal Raphe Dopamine Neurons Modulate Arousal and Promote Wakefulness by Salient Stimuli**. *Neuron* 2017, **94**(6):1205-1219.e1208.
23. Bliss TV, Collingridge GL, Kaang BK, Zhuo M: **Synaptic plasticity in the anterior cingulate cortex in acute and chronic pain**. *Nat Rev Neurosci* 2016, **17**(8):485-496.
24. Villarreal CF, Del Bel EA, Prado WA: **Involvement of the anterior pretectal nucleus in the control of persistent pain: a behavioral and c-Fos expression study in the rat**. *Pain* 2003, **103**(1-2):163-174.
25. Cheriyan J, Sheets PL: **Altered Excitability and Local Connectivity of mPFC-PAG Neurons in a Mouse Model of Neuropathic Pain**. *J Neurosci* 2018, **38**(20):4829-4839.

26. Yeung JC, Yaksh TL, Rudy TA: **Concurrent mapping of brain sites for sensitivity to the direct application of morphine and focal electrical stimulation in the production of antinociception in the rat**. *Pain* 1977, **4**(1):23-40.

27. Llorca-Torralba M, Camarena-Delgado C, Suárez-Pereira I, Bravo L, Mariscal P, Garcia-Partida JA, López-Martín C, Wei H, Pertovaara A, Mico JA *et al*: **Pain and depression comorbidity causes asymmetric plasticity in the locus coeruleus neurons**. *Brain* 2021, **145**(1):154-167.

28. Duncan GE, Moy SS, Knapp DJ, Mueller RA, Breese GR: **Metabolic mapping of the rat brain after subanesthetic doses of ketamine: potential relevance to schizophrenia**. *Brain Res* 1998, **787**(2):181-190.

29. Ma S, Allocca G, Ong-Pålsson EK, Singleton CE, Hawkes D, McDougall SJ, Williams SJ, Bathgate RA, Gundlach AL: **Nucleus incertus promotes cortical desynchronization and behavioral arousal**. *Brain Struct Funct* 2017, **222**(1):515-537.

30. Musacchio T, Rebenstorff M, Fluri F, Brotchie JM, Volkmann J, Koprich JB, Ip CW: **Subthalamic nucleus deep brain stimulation is neuroprotective in the A53T α-synuclein Parkinson's disease rat model**. *Ann Neurol* 2017, **81**(6):825-836.

31. Hauer BE, Pagliardini S, Dickson CT: **Prefrontal-Hippocampal Pathways Through the Nucleus Reuniens Are Functionally Biased by Brain State**. *Front Neuroanat* 2021, **15**:804872.

32. Deng J, Zhou H, Lin JK, Shen ZX, Chen WZ, Wang LH, Li Q, Mu D, Wei YC, Xu XH *et al*: **The Parabrachial Nucleus Directly Channels Spinal Nociceptive Signals to the Intralaminar Thalamic Nuclei, but Not the Amygdala**. *Neuron* 2020, **107**(5):909-923 e906.

33. Bekkers JM, Suzuki N: **Neurons and circuits for odor processing in the piriform cortex**. *Trends Neurosci* 2013, **36**(7):429-438.

34. Xu W, Wilson DA: **Odor-evoked activity in the mouse lateral entorhinal cortex**. *Neuroscience* 2012, **223**:12-20.

35. Gupta RG, Schafer C, Ramaroson Y, Sciullo MG, Horn CC: **Role of the abdominal vagus and hindbrain in inhalational anesthesia-induced vomiting**. *Auton Neurosci* 2017, **202**:114-121.

36. Yi T, Wang N, Huang J, Wang Y, Ren S, Hu Y, Xia J, Liao Y, Li X, Luo F *et al*: **A Sleep-Specific Midbrain Target for Sevoflurane Anesthesia**. *Adv Sci (Weinh)* 2023:e2300189.

37. Wheeler AL, Teixeira CM, Wang AH, Xiong X, Kovacevic N, Lerch JP, McIntosh AR, Parkinson J, Frankland PW: **Identification of a functional connectome for long-term fear memory in mice**. *PLoS Comput Biol* 2013, **9**(1):e1002853.

38. Power JD, Schlaggar BL, Lessov-Schlaggar CN, Petersen SE: **Evidence for hubs in human functional brain networks**. *Neuron* 2013, **79**(4):798-813.

39. Meunier D, Achard S, Morcom A, Bullmore E: **Age-related changes in modular organization of human brain functional networks**. *NeuroImage* 2009, **44**(3):715-723.

40. Zerbi V, Floriou-Servou A, Markicevic M, Vermeiren Y, Sturman O, Privitera M, von Ziegler L, Ferrari KD, Weber B, De Deyn PP *et al*: **Rapid Reconfiguration of the Functional Connectome after Chemogenetic Locus Coeruleus Activation**. *Neuron* 2019, **103**(4):702-718 e705.

41. Vierck CJ, Whitsel BL, Favorov OV, Brown AW, Tommerdahl M: **Role of primary somatosensory cortex in the coding of pain**. *Pain* 2013, **154**(3):334-344.

42. Cichon J, Wasilczuk AZ, Looger LL, Contreras D, Kelz MB, Proekt A: **Ketamine triggers a switch in excitatory neuronal activity across neocortex**. *Nat Neurosci* 2022.

43. Rubinov M, Sporns O: **Complex network measures of brain connectivity: uses and interpretations**. *NeuroImage* 2010, **52**(3):1059-1069.

44. Shannon P, Markiel A, Ozier O, Baliga NS, Wang JT, Ramage D, Amin N, Schwikowski B, Ideker T: **Cytoscape: a software environment for integrated models of biomolecular interaction networks**. *Genome Res* 2003, **13**(11):2498-2504.

45. Guimera R, Nunes Amaral LA: **Functional cartography of complex metabolic networks**. *Nature* 2005, **433**(7028):895-900.

46. Newman ME: **Modularity and community structure in networks**. *Proceedings of the National Academy of Sciences of the United States of America* 2006, **103**(23):8577-8582.

47. Reimann HM, Niendorf T: **The (Un)Conscious Mouse as a Model for Human Brain Functions: Key Principles of Anesthesia and Their Impact on Translational Neuroimaging**. *Front Syst Neurosci* 2020, **14**:8.

48. Nagata A, Nakao S, Miyamoto E, Inada T, Tooyama I, Kimura H, Shingu K: **Propofol inhibits ketamine-induced c-fos expression in the rat posterior cingulate cortex**. *Anesth Analg* 1998, **87**(6):1416-1420.

49. Nagata A, Nakao Si S, Nishizawa N, Masuzawa M, Inada T, Murao K, Miyamoto E, Shingu K: **Xenon inhibits but N(2)O enhances ketamine-induced c-Fos expression in the rat posterior cingulate and retrosplenial cortices**. *Anesth Analg* 2001, **92**(2):362-368.

50. Inta D, Trusel M, Riva MA, Sprengel R, Gass P: **Differential c-Fos induction by different NMDA receptor antagonists with antidepressant efficacy: potential clinical implications**. *Int J Neuropsychopharmacol* 2009, **12**(8):1133-1136.

51. Nakao S, Arai T, Mori K, Yasuhara O, Tooyama I, Kimura H: **High-dose ketamine does not induce c-Fos protein expression in rat hippocampus**. *Neurosci Lett* 1993, **151**(1):33-36.

52. Nakao S, Miyamoto E, Masuzawa M, Kambara T, Shingu K: **Ketamine-induced c-Fos expression in the mouse posterior cingulate and retrosplenial cortices is mediated not only via NMDA receptors but also via sigma receptors**. *Brain Res* 2002, **926**(1-2):191-196.

53. Hase T, Hashimoto T, Saito H, Uchida Y, Kato R, Tsuruga K, Takita K, Morimoto Y: **Isoflurane induces c-Fos expression in the area postrema of the rat**. *Journal of anesthesia* 2019, **33**(4):562-566.

Supplementary Information

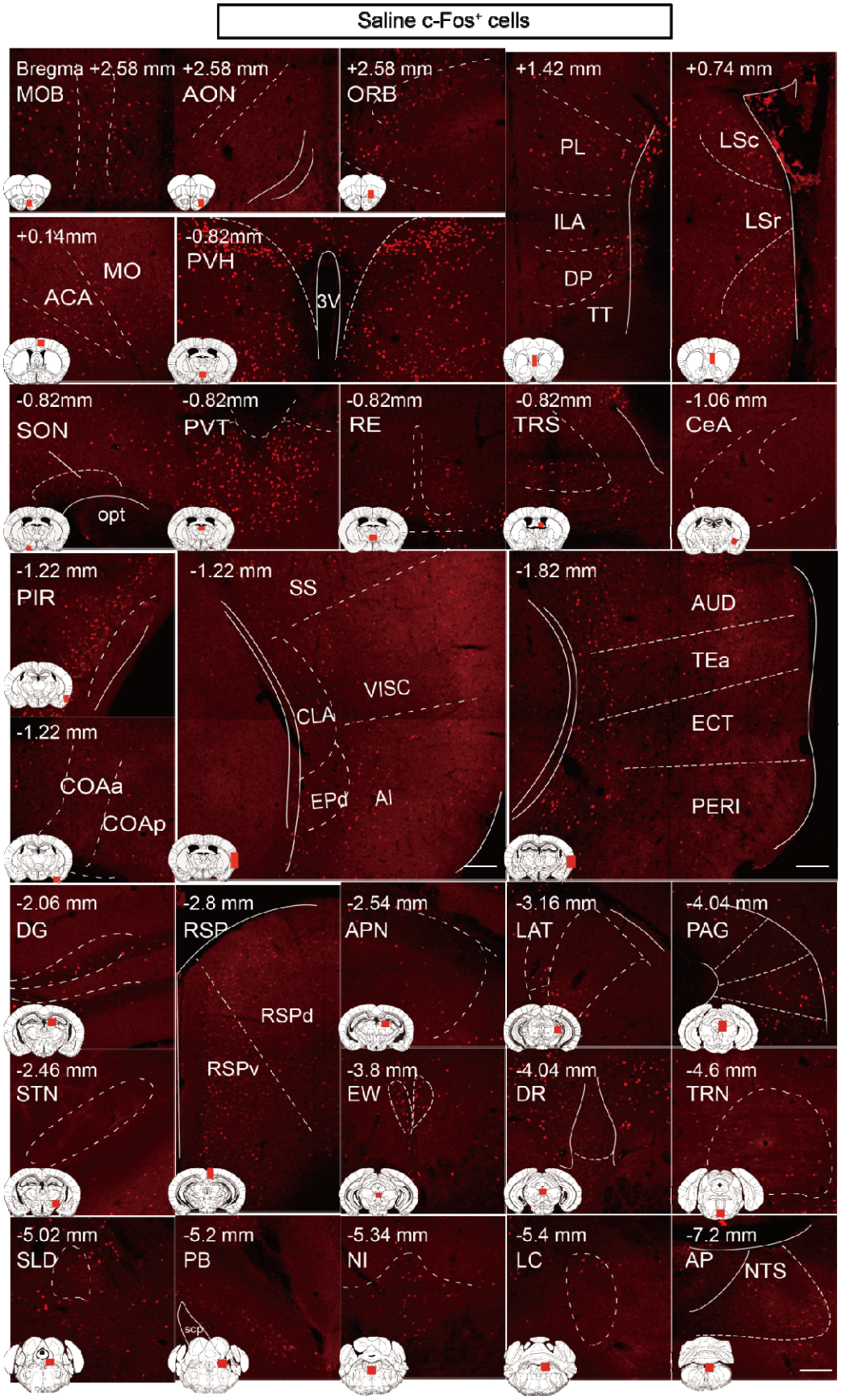

Supplementary Figure 1. c-Fos expression in distinct brain regions after exposure to normal saline administration. (A) Representative immunohistochemical staining of MOB, AON, ORB, MPO, ACA, MO, TRS, PL, ILA, DP, LS, PVT, SON, PVH, RE, VISC, AI, CLA, EPd, PIR, COA, AUD, TEa, ECT, PERI, CeA, SS, DG, STN, RSP, APN, LAT, EW, DR, PAG, SLD, PB, TRN, NI, LC, and NTS c-Fos$^+$ cells from the indicated mice. Scale bar, 200 μm.

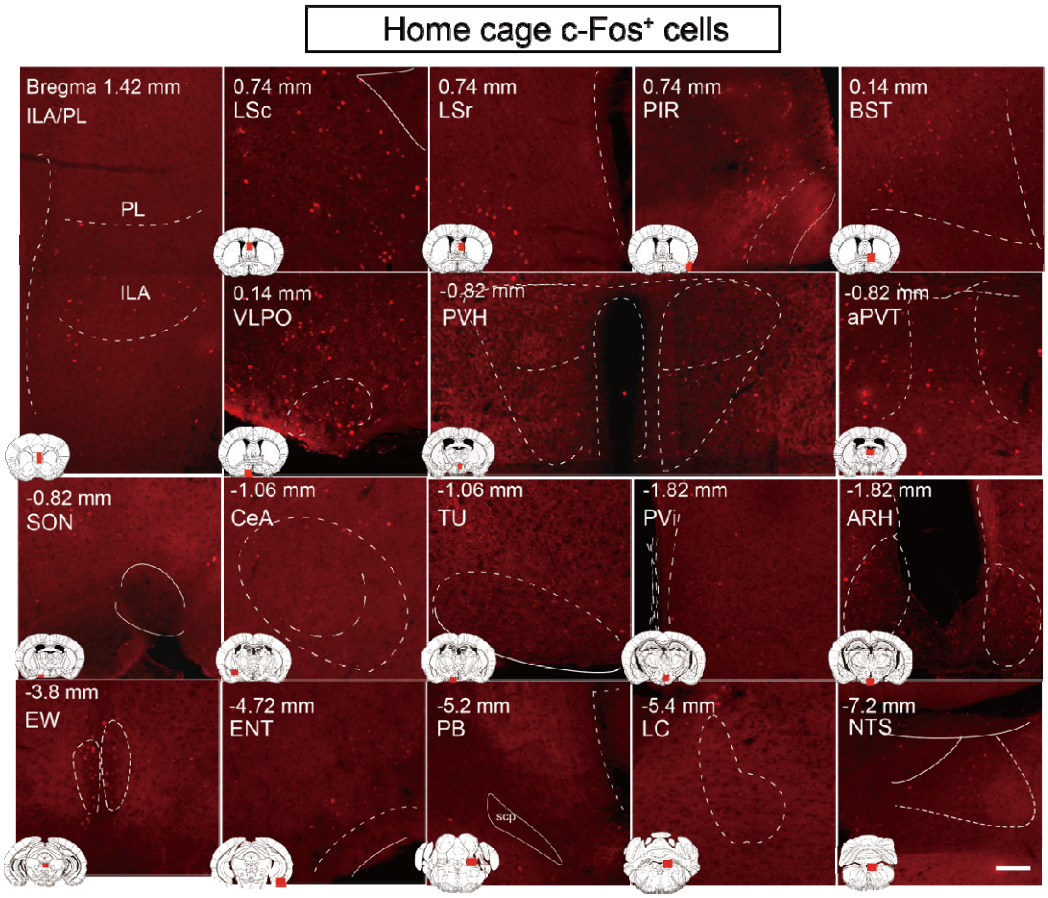

Supplementary Figure 2. c-Fos expression in home cage group.

(A) Representative immunohistochemical staining of PL, ILA, LSc, LSr, PIR, BST, VLPO, PVH, aPVT, SON, CeA, TU, PVi, ARH, EW, ENT, PB, LC, and NTS c-Fos$^+$ cells from the indicated mice. Scale bar, 200 μm.

Supplementary Table 1. Distribution of c-Fos$^+$ cells in 53 brain areas for the home cage, ISO, Saline, and KET groups.

Brain Structure	Substructure	Abbreviation	Home cage	ISO	Saline	KET
Pallidum	Pallidum,dorsal region	PALd	0.057±0.028	0.010±0.005	0.080±0.048	0.131±0.065
	Pallidum,ventral region	PALv	0.253±0.083	0.712±0.093	0.363±0.157	0.785±0.106
	Pallidum,medial region	PALm	0.311±0.096	0.575±0.054	0.305±0.080	0.511±0.060
	Pallidum,caudal region	PALc	1.108±0.184	3.648±0.356	0.626±0.186	0.402±0.107
Striatum	Striatum dorsal region	STRd	0.500±0.126	0.572±0.183	1.191±0.543	3.466±0.840
	Striatum ventral region	STRv	0.589±0.098	2.774±0.402	0.597±0.267	2.312±0.287
	Lateral septal complex	LSX	1.932±0.586	5.108±0.413	2.285±0.610	1.052±0.059
	Striatum-like amygdalar nuclei	sAMY	1.135±0.376	6.541±0.541	1.830±0.417	0.952±0.283
Olfactory areas	Main olfactory bulb	MOB	0.677±0.292	1.702±0.517	1.420±0.791	2.792±1.255
	Accessory olfactory bulb	AOB	0.109±0.066	0.208±0.139	0.178±0.093	0.419±0.228
	Anterior olfactory nucleus	AON	0.999±0.548	1.117±0.354	1.053±0.486	2.376±0.681
	Taenia tecta	TT	0.469±0.099	1.193±0.274	0.463±0.280	0.700±0.254
	Dorsal peduncular area	DP	0.020±0.009	0.171±0.047	0.075±0.035	0.162±0.044
	Piriform area	PIR	1.300±0.356	4.166±1.449	3.248±0.528	4.515±0.747
	Nucleus of the lateral olfactory tract	NLOT	0.097±0.044	0.091±0.040	0.240±0.120	0.090±0.029
	Cortical amygdalar area	COA	0.365±0.114	0.430±0.096	1.140±0.193	0.878±0.210
	Piriform-amygdalar area	PAA	0.063±0.018	0.120±0.040	0.336±0.076	0.213±0.049
	Post piriform transition area	TR	0.324±0.131	0.130±0.058	0.350±0.089	0.325±0.072
Isocortex	*Somatomotor areas*	*MO*	*0.736±0.22*	*0.263±0.10*	*0.715±0.22*	*4.671±0.24*

			5	*5*	*5*	*4*
	Somatosensory areas	SS	0.775±0.309	0.231±0.123	1.058±0.489	9.487±1.551
	Gustatory areas	GU	0.032±0.019	0.048±0.018	0.040±0.017	0.288±0.044
	Visceral area	VISC	0.014±0.007	0.004±0.003	0.147±0.071	0.564±0.142
	Auditory areas	AUD	0.256±0.093	0.246±0.081	1.481±0.427	2.267±0.198
	Visual areas	VIS	0.501±0.247	0.189±0.044	4.503±1.343	7.013±0.775
	Anterior cingulate area	ACA	0.183±0.078	0.146±0.037	0.736±0.337	2.179±0.145
	Prelimbic area	PL	0.118±0.043	0.160±0.053	0.283±0.100	0.649±0.086
	Infralimbic area	ILA	0.279±0.056	0.922±0.144	0.409±0.182	0.615±0.217
	Orbital area	ORB	0.337±0.083	0.393±0.054	0.453±0.167	1.759±0.152
	Agranular insular area	AI	0.146±0.047	0.096±0.032	0.533±0.164	1.475±0.231
	Retrosplenial area	RSP	1.007±0.349	0.552±0.114	2.455±0.721	5.070±0.773
	Posterior parietal association areas	PTLp	0.149±0.032	0.035±0.016	0.238±0.111	0.598±0.359
	Temporal association areas	TEa	0.266±0.104	0.513±0.194	1.501±0.433	1.539±0.135
	Ectorhinal area	ECT	0.305±0.144	0.901±0.384	1.507±0.341	1.301±0.341
	Frontal Pole, cerebral cortex	FRP	0.020±0.013	0.030±0.027	0.074±0.043	0.029±0.012
Hippocampal formation	Hippocampal region	HIP	4.240±1.230	3.531±0.843	4.281±0.766	2.938±0.469
	Retrohippocampal region	RHP	1.689±0.500	3.558±1.068	4.627±1.113	9.551±0.967
Cortical subplate	Cortical subplate	CTXsp	1.122±0.216	0.910±0.181	2.798±0.440	2.410±0.226
Thalamus	Thalamus, sensory motor cortex-related	DORsm	0.881±0.160	0.505±0.185	0.779±0.102	0.546±0.082
	Thalamus, polymodal association cortex-related	DORpm	7.353±1.042	6.104±0.601	4.674±0.992	3.502±0.259

Hypothal-amus	Periventricular zone	PVZ	2.330±0.759	6.627±0.843	1.306±0.345	0.334±0.068
	Periventricular region	PVR	9.800±2.909	8.145±0.869	3.140±0.421	0.762±0.088
	Hypothalamic medial zone	MEZ	6.198±1.192	3.878±0.204	5.121±0.832	1.349±0.174
	Hypothalamic lateral zone	LZ	2.815±0.304	5.589±0.752	2.606±0.718	0.883±0.167
Midbrain	Midbrain, sensory-related	MBsen	11.525±3.354	2.449±0.735	7.507±2.343	1.466±0.332
	Midbrain, motor-related	MBmot	10.099±1.299	4.515±1.105	11.659±1.716	3.712±0.588
	Midbrain, behavioral state-related	MBsta	0.471±0.125	0.535±0.145	0.834±0.168	0.380±0.099
Pons	Pons, sensory-related	P-sen	1.729±0.917	0.806±0.261	0.842±0.149	0.661±0.231
	Pons, motor-related	P-mot	3.579±1.115	0.715±0.197	2.772±0.562	1.168±0.247
	Pons, behavioral state-related	P-sat	0.816±0.314	0.572±0.115	1.286±0.308	0.564±0.109
Medulla	Medulla, sensory-related	MY-sen	0.618±0.241	2.042±0.426	0.700±0.249	0.356±0.098
	Medulla, motor-related	MY-mot	3.410±1.727	1.542±0.144	1.347±0.369	1.476±0.374
	Medulla, behavioral state-related	MY-sat	0.020±0.013	0.019±0.008	0.024±0.011	0.078±0.032
Cerebel-lum	Cerebellum	CB	3.451±1.469	1.379±0.352	1.869±0.611	0.508±0.245

Shown are the mean ± SEM. of the percentage of c-Fos$^+$ cells in each area.

Supplementary Table 2. Sum of previous studies on ketamine activated brain regions detected by c-Fos immunostaining.

Brain regions	Function	Treatment Reg-imen	Dura-tion	Time of day	Effect	References
CeA	Pain Suppression	100mg/kg and 10mg/kgxylazine i.p.	2h	/	Up-regulated	Hua T, et al.,(2022) [17]
SON	Natural sleep/General an-esthesia	100mg/kg with or without xylazine(10mg/k	2h	/	Up-regulated	Jiang-Xie LF, et al.,(2019) [18]

		g) i.p				
pCC	/	100mg/kg i.p.	2h	/	Up-regulated	Nagata A, et al.,(1998) [48]
pCC, RSC	/	100mg/kg i.p.	2h	/	Up-regulated	Nagata A, et al.,(2001) [49]
RSP, CeA, Midline thalamic nuclei	Antidepressant	10mg/kg i.p.	1.5h	/	Up-regulated	Inta D, et al.,(2009) [50]
Cg, BF, Orx, TMN, vlPAG, LC, LHb, EW, mid-line thal-amus	LC/vPAG engaged in analgesia	150mg/kg, 60mg/kg, 30mg/kg i.p.	2h	ZT3	Up-regulated	Lu J, et al.,(2008) [13]
CC, PVT	/	100mg/kg i.p.	/	/	/	Nakao S, et al.,(1993) [51]
PC, RSP	/	50mg/kg i.p.	2h	ZT3-9	Up-regulated	Nakao S, et al.,(2002) [52]

Abbreviation: CeA, Central amygdalar nucleus; SON, Supraoptic nucleus; pCC, Posterior cingulate cortex; RSC, Retrosplenial cortex; RSP, Retrosplenial area; Cg, cingulate cortex; BF, basal forebrain cholinergic cells; Orx, perifornical orexin cells; vlPAG, ventrolateral periaquductal gray dopa-mine cells; LC, Locus coeruleus; LHb, lateral habenular nucleus; EW, Edinger-Westphal nucleus; CC, Cerebral cortex; PVT, Paraventricular nucleus of the thalamus; PC, posterior cingulate. RSP, Retrosplenial area.

Supplementary Table 3. The sum of previous studies on isoflurane acti-vated brain regions detected by c-Fos immunostaining.

Brain regions	Function	Concentra-tion of ISO	Dura-tion	Time of day		References
VLPO	Sleep-Promoting, Hypnosis	1.2%, 0.6%, 0.3%	2h	ZT12-14/ZT4-6	Up-regulated	Moore JT,.et al.,(2012) [7]
PIR, LSD,	/	4% 5mins+1%	2h	ZT2-7	Up-regulated	Smith ML, et al.,(2016) [12]

LSV						
NTS, VeN	Vomiting	1% and 3%	1.5h	/	Up-regulated	Gupta RG, et al.,(2016) [35]
CeA	Pain Suppression	1.5%	2h	/	Up-regulated	Hua T, et al.,(2022) [17]
SON	Natural sleep, General anesthesia	1%,1.2%	2h	/	Up-regulated	Jiang-Xie LF, et al.,(2019) [18]
VLPO, MnPO	Sleep and uncon-sciousness	1.2%	2h	ZT14-17	Up-regulated	Han B, et al.,(2022) [15]
EW, VLPO, LC	Sleep-Promoting, analgesia	2%	2h	ZT12	Up-regulated	Lu J, et al.,(2008) [13]
AP	Nausea, vomiting	1.3%,2.6%	2h	/	Up-regulated	Hase T, et al.,(2019) [53]

Abbreviation: VLPO, Ventrolateral preoptic nucleus; PIR, Piriform area; LSD, Lateral septal nucleus, dorsal part; LSV, Lateral septal nucleus, ventral part; NTS, Nucleus of the solitary tract; VeN, Ventral group of the dorsal thalamus; CeA, Central amygdalar nucleus; SON, Supraoptic nucleus; MnPO, median preoptic nucleus; EW, Edinger-Westphal nucleus; LC, Locus coeruleus; AP, Area postrema.

Supplementary Table 4. Abbreviations of the relevant brain regions in Figure 3.

Region	Abbreviation	Region	Abbreviation	Re-gion	Abbreviation
CTX	**Cerebral cortex**	LH	Lateral habenula	OP	Olivary pretectal nucleus
PA	Posterior amygdalar nucle-us	SPF	Subparafascicular nucle-us	ND	Nucleus of Darkschewitsch
PIR	Piriform area	MH	Medial habenula	VTN	Ventral tegmental nucleus
DG	Dentate gyrus	ATN	Anterior group of the dorsal thalamus	IF	Interfascicular nucleus raphe
ENT	Entorhinal area	VENT	Ventral group of the dor-sal thalamus	PPT	Posterior pretectal nucleus
MOB	Main olfactory bulb	LAT	Lateral group of the dor-sal thalamus	MRNm	Midbrain reticular nucleus, magnocellular part
CA	Ammon's horn	GENd	Geniculate group, dorsal thalamus	MRNmg	Midbrain reticular nucleus, magnocellular part, general

AON	Anterior olfactory nucleus	RT	Reticular nucleus of the thalamus	MRNp	Midbrain reticular nucleus, parvicellular part
TT	Taenia tecta	SPA	Subparafascicular area	INC	Interstitial nucleus of Cajal
ECT	Ectorhinal area	PP	Peripeduncular nucleus	CS	Superior central nucleus raphe
RSP	Retrosplenial area	PIN	Pineal body	**HB**	**Hindbrain**
ILA	Infralimbic area	**HY**	**Hypothalamus**	NTS	Nucleus of the solitary tract
SUB	Subiculum	SO	Supraoptic nucleus	PB	Parabrachial nucleus
TEa	Temporal association areas	PVH	Paraventricular hypothalamic nucleus	PG	Pontine gray
COA	Cortical amygdalar area	LHA	Lateral hypothalamic area	VNC	Vestibular nuclei
ORB	Orbital area	MPO	Medial preoptic area	GRN	Gigantocellular reticular nucleus
SS	Somatosensory areas	AHN	Anterior hypothalamic nucleus	LRN	Lateral reticular nucleus
MO	Somatomotor areas	SBPV	Subparaventricular zone	PCG	Pontine central gray
VIS	Visual areas	DMH	Dorsomedial nucleus of the hypothalamus	PRNc	Pontine reticular nucleus, caudal part
PERI	Perirhinal area	TU	Tuberal nucleus	IRN	Intermediate reticular nucleus
AUD	Auditory areas	SCH	Suprachiasmatic nucleus	MDRN	Medullary reticular nucleus
AOB	Accessory olfactory bulb	PH	Posterior hypothalamic nucleus	AP	Area postrema
EP	Endopiriform nucleus	ARH	Arcuate hypothalamic nucleus	PRNr	Pontine reticular nucleus
BMAp	Basomedial amygdalar nucleus, posterior part	LPO	Lateral preoptic area	NLL	Nucleus of the lateral lemniscus
TR	Postpiriform transition area	RCH	Retrochiasmatic area	DMX	Dorsal motor nucleus of the vagus nerve
BLA	Basolateral amygdalar nucleus	VMH	Ventromedial hypothalamic nucleus	TRN	Tegmental reticular nucleus
PL	Prelimbic area	VLPO	Ventrolateral preoptic nucleus	CN	Cochlear nuclei
ACA	Anterior cingulate area	PVpo	Periventricular hypothalamic nucleus, preoptic part	DCN	Dorsal column nuclei
LA	Lateral	MPN	Medial preoptic nucleus	PAS	Parasolitary nucleus

	amygdalar nucleus				
DP	Dorsal peduncular area	PVi	Periventricular hypothalamic nucleus, intermediate part	PGRN	Paragigantocellular reticular nucleus
PAA	Piriform-amygdalar area	ZI	Zona incerta	PARN	Parvicellular reticular nucleus
POST	Postsubiculum	MEPO	Median preoptic nucleus	LC	Locus ceruleus
AI	Agranular insular area	AVPV	Anteroventral periventricular nucleus	SPVI	Spinal nucleus of the trigeminal, interpolar part
BMAa	Basomedial amygdalar nucleus, anterior part	MBO	Mammillary body	PHY	Perihypoglossal nuclei
PAR	Parasubiculum	PVa	Periventricular hypothalamic nucleus, anterior part	NI	Nucleus incertus
NLOT	Nucleus of the lateral olfactory tract	PVHd	Paraventricular hypothalamic nucleus, descending division	LDT	Laterodorsal tegmental nucleus
PRE	Presubiculum	PSTN	Parasubthalamic nucleus	V	Motor nucleus of trigeminal
PTLp	Posterior parietal association areas	PVp	Periventricular hypothalamic nucleus, posterior part	DTN	Dorsal tegmental nucleus
GU	Gustatory areas	ADP	Anterodorsal preoptic nucleus	B	Barrington's nucleus
CLA	Claustrum	PMv	Ventral premammillary nucleus	SPVC	Spinal nucleus of the trigeminal, caudal part
FRP	Frontal pole, cerebral cortex	AVP	Anteroventral preoptic nucleus	MARN	Magnocellular reticular nucleus
IG	Induseum griseum	PMd	Dorsal premammillary nucleus	XII	Hypoglossal nucleus
VISC	Visceral area	PS	Parastrial nucleus	SOC	Superior olivary complex
6b	Layer 6b, isocortex	OV	Vascular organ of the lamina terminalis	SLD	Sublaterodorsal nucleus
FC	Fasciola cinerea	STN	Subthalamic nucleus	AMB	Nucleus ambiguus
CNU	**Cerebral nuclei**	SFO	Subfornical organ	VII	Facial motor nucleus
BST	Bed nuclei of the stria terminalis	PD	Posterodorsal preoptic nucleus	NTB	Nucleus of the trapezoid body
CEA	Central amygdalar nucleus	PST	Preparasubthalamic nucleus	SPVO	Spinal nucleus of the trigeminal, oral part
LSr	Lateral septal	ASO	Accessory supraoptic	RPO	Nucleus raphe pontis

	nucleus, rostral (rostroventral) part		group		
SI	Substantia innominata	AHA	Anterior hypothalamic area	RO	Nucleus raphe obscurus
NDB	Diagonal band nucleus	PSCH	Suprachiasmatic preoptic nucleus	IO	Inferior olivary complex
ACB	Nucleus accumbens	IPN	Interpeduncular nucleus	SUT	Supratrigeminal nucleus
MS	Medial septal nucleus	**MB**	**Midbrain**	RM	Nucleus raphe magnus
OT	Olfactory tubercle	ICc	Inferior colliculus, central nucleus	LIN	Linear nucleus of the medulla
LSc	Lateral septal nucleus, caudal (caudodorsal) part	SCsg	Superior colliculus, superficial gray layer	x	Nucleus x
AAA	Anterior amygdalar area	ICe	Inferior colliculus, external nucleus	PSV	Principal sensory nucleus of the trigeminal
FS	Fundus of striatum	SCig	Superior colliculus, motor related, intermediate gray layer	y	Nucleus y
MA	Magnocellular nucleus	ICd	Inferior colliculus, dorsal nucleus	SLC	Subceruleus nucleus
IA	Intercalated amygdalar nucleus	SCzo	Superior colliculus, zonal layer	ECU	External cuneate nucleus
MEA	Medial amygdalar nucleus	SCdg	Superior colliculus, motor related, deep gray layer	VI	Abducens nucleus
CP	Caudoputamen	SCop	Superior colliculus, optic layer	RPA	Nucleus raphe pallidus
SF	Septofimbrial nucleus	EW	Edinger-Westphal nucleus	LTN	Lateral tegmental nucleus
BA	Bed nucleus of the accessory olfactory tract	PRC	Precommissural nucleus	PRNv	Pontine reticular nucleus, ventral part
SH	Septohippocampal nucleus	SCiw	Superior colliculus, motor related, intermediate white layer	SG	Supragenual nucleus
GPe	Globus pallidus, external segment	MPT	Medial pretectal area	SSN	Superior salivatory nucleus
TRS	Triangular nucle-	VTA	Ventral tegmental area	z	Nucleus z

	us of septum				
BAC	Bed nucleus of the anterior commissure	DR	Dorsal nucleus raphe	ACVI	Accessory abducens nucleus
GPi	Globus pallidus, internal segment	NPC	Nucleus of the posterior commissure	ACVII	Accessory facial motor nucleus
LSv	Lateral septal nucleus, ventral part	APN	Anterior pretectal nucleus	EV	Efferent vestibular nucleus
PVT	Paraventricular nucleus of the thalamus	SNr	Substantia nigra, reticular part	ECO	Efferent cochlear group
TH	**Thalamus**	NOT	Nucleus of the optic tract	ICB	Infracerebellar nucleus
RE	Nucleus of reunions	CLI	Central linear nucleus raphe	ISN	Inferior salivatory nucleus
GENv	Geniculate group, ventral thalamus	RL	Rostral linear nucleus raphe	PMR	Paramedian reticular nucleus
ILM	Intralaminar nuclei of the dorsal thalamus	SNc	Substantia nigra, compact part	PPY	Parapyramidal nucleus
PT	Parataenial nucleus	SCdw	Superior colliculus, motor related, deep white layer	INV	Interstitial nucleus of the vestibular nerve
MED	Medial group of the dorsal thalamus	RN	Red nucleus	SIMmo	Simple lobule, molecular layer

Supplementary Table 5. The brain regions used for functional network analysis in Figure 6.

	CTX	Cerebral cortex		HY	Hypothalamus
1	ACA	Anterior cingulate area	32	ARH	Arcuate hypothalamic nucleus
2	AI	Agranular insular area	33	LHA	Lateral hypothalamic area
3	AUD	Auditory areas	34	LPO	Lateral preoptic area
4	CA	Ammon's horn	35	MBO	Mammillary body
5	COA	Cortical amygdalar area	36	MEPO	Median preoptic nucleus
6	DG	Dentate gyrus	37	MPN	Medial preoptic nucleus
7	ECT	Ectorhinal area	38	MPO	Medial preoptic area
8	ENT	Entorhinal area	39	PVH	Paraventricular hypothalamic nucleus
9	ILA	Infralimbic area	40	PVi	Periventricular hypothalamic nucleus, intermediate part
10	MO	Somatomotor areas	41	SO	Supraoptic nucleus

11	MOB	Main olfactory bulb	42	STN	Subthalamic nucleus
12	ORB	Orbital area	43	TU	Tuberal nucleus
13	PIR	Piriform area	44	VLPO	Ventrolateral preoptic nucleus
14	PL	Prelimbic area	45	ZI	Zona incerta
15	RSP	Retrosplenial area		MB	Midbrain
16	SS	Somatosensory areas	46	APN	Anterior pretectal nucleus
17	TEa	Temporal association areas	47	DR	Dorsal nucleus raphe
18	TT	Taenia tecta	48	EW	Edinger-Westphal nucleus
19	VIS	Visual areas	49	PAG	Periaqueductal gray
	CNU	Cerebral nuclei	50	RR	Midbrain reticular nucleus, retrorubral area
20	ACB	Nucleus accumbens	51	SNr	Substantia nigra, reticular part
21	BST	Bed nuclei of the stria terminalis	52	VTA	Ventral tegmental area
22	CEA	Central amygdalar nucleus	53	MRN	Midbrain reticular nucleus
23	LSc	Lateral septal nucleus, caudal (caudodorsal) part	54	PPN	Pedunculopontine nucleus
24	LSr	Lateral septal nucleus, rostral (rostroventral) part		HB	Hindbrain
25	OT	Olfactory tubercle	55	CS	Superior central nucleus raphe
26	MS	Medial septal nucleus	56	LC	Locus ceruleus
	TH	Thalamus	57	NTS	Nucleus of the solitary tract
27	LAT	Lateral group of the dorsal thalamus	58	PB	Parabrachial nucleus
28	LH	Lateral habenula	59	PCG	Pontine central gray
29	PVT	Paraventricular nucleus of the thalamus	60	SLD	Sublaterodorsal nucleus
30	RE	Nucleus of reunions	61	TRN	Tegmental reticular nucleus
31	RT	Reticular nucleus of the thalamus	62	LDT	Laterodorsal tegmental nucleus
			63	PRNr	Pontine reticular nucleus（PRNr）

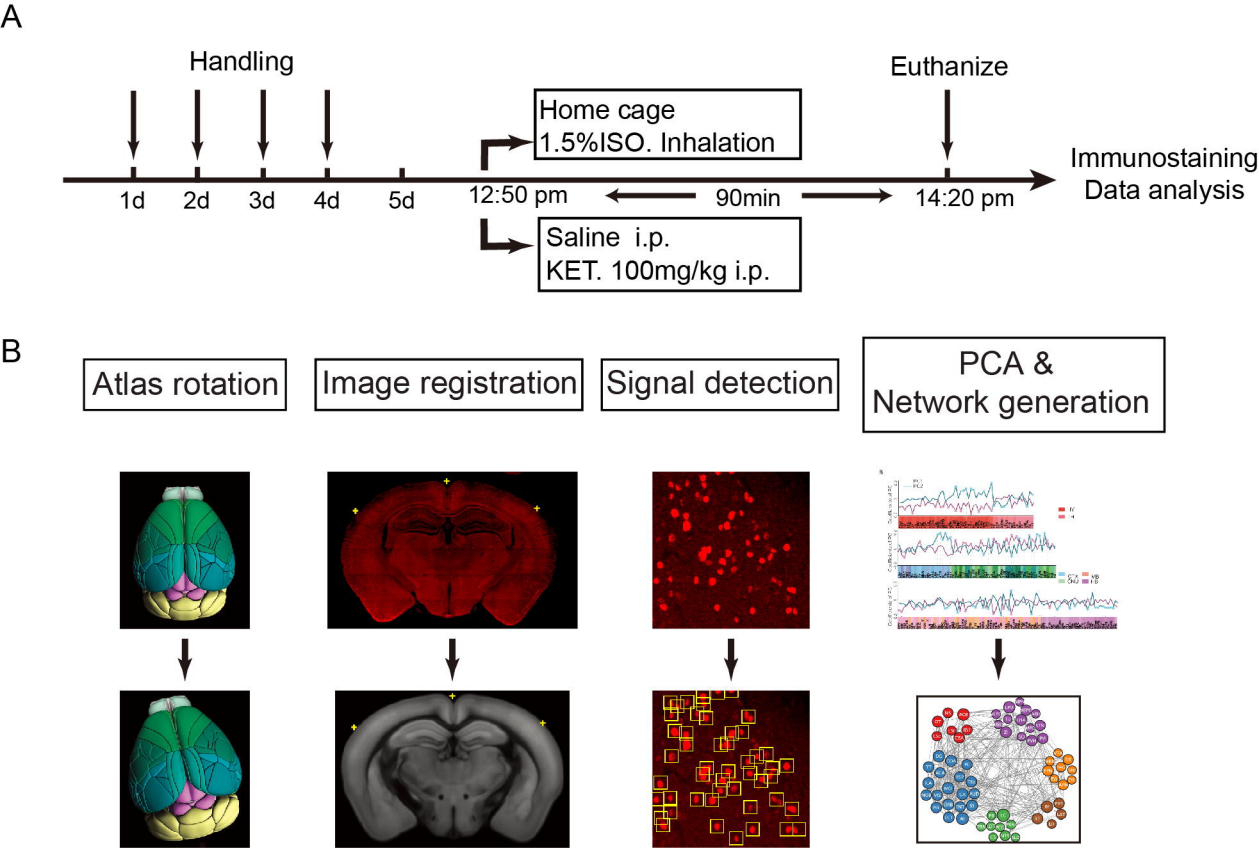
A
Handling
Euthanize
Home cage
1.5%ISO. Inhalation
1d
2d
3d
4d
5d
12:50 pm
90min
14:20 pm
Immunostaining
Data analysis
Saline i.p.
KET. 100mg/kg i.p.
B
Atlas rotation
Image registration
Signal detection
PCA &
Network generation

A

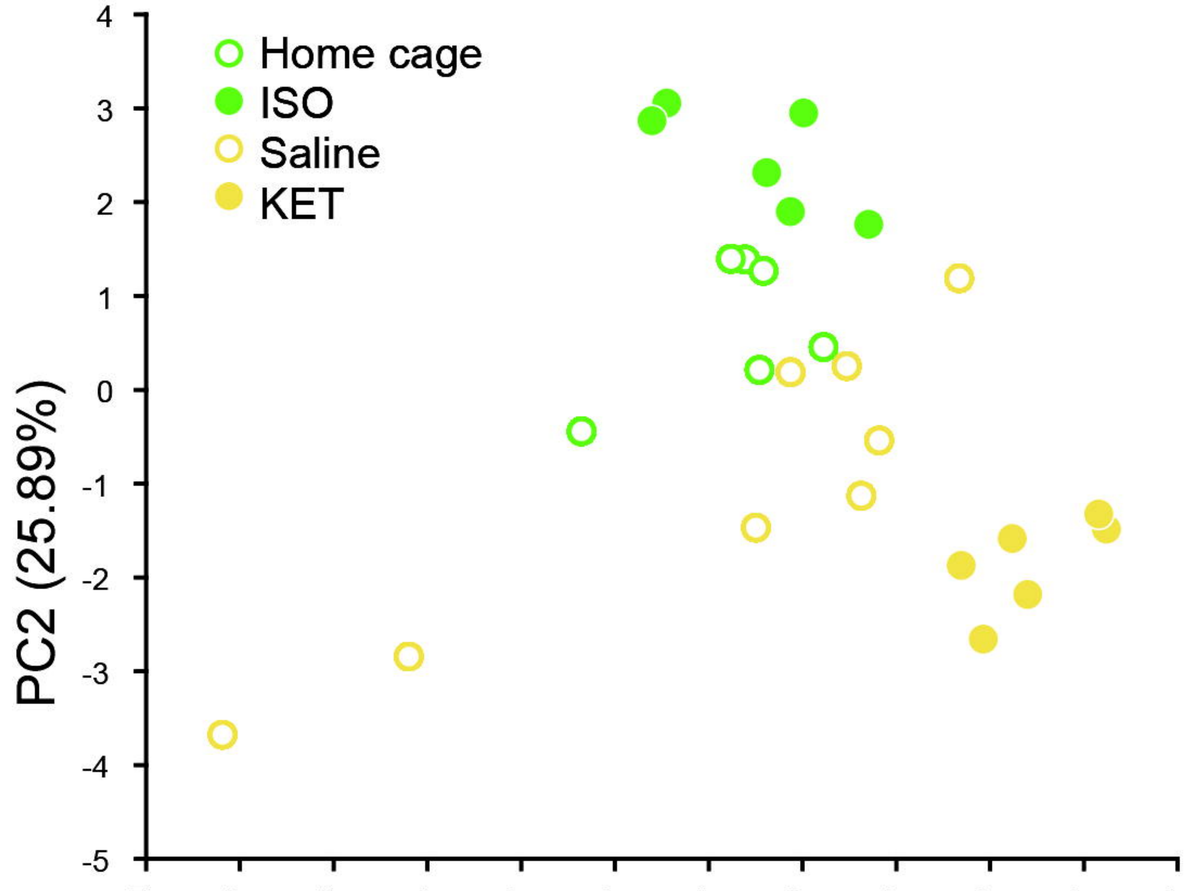

B

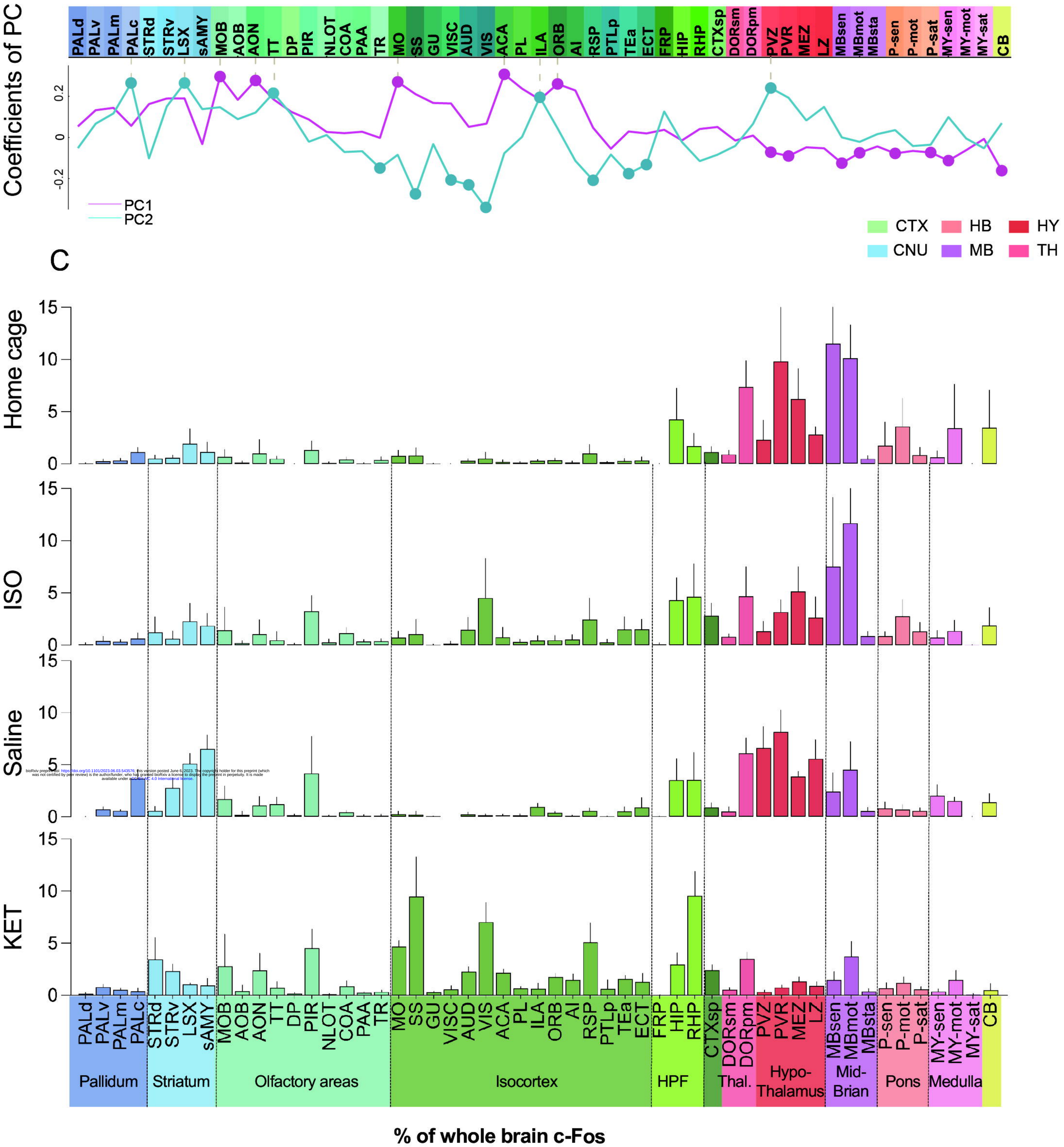

C

A

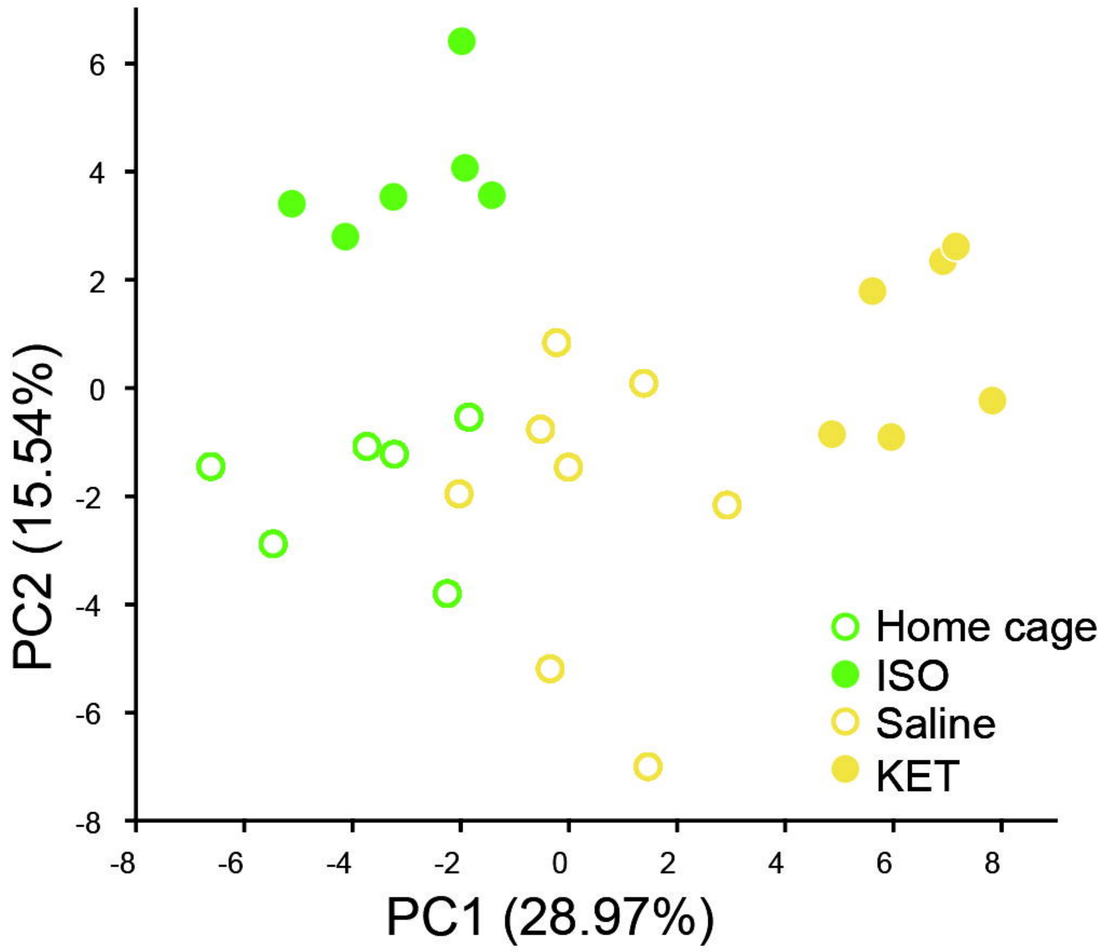

C

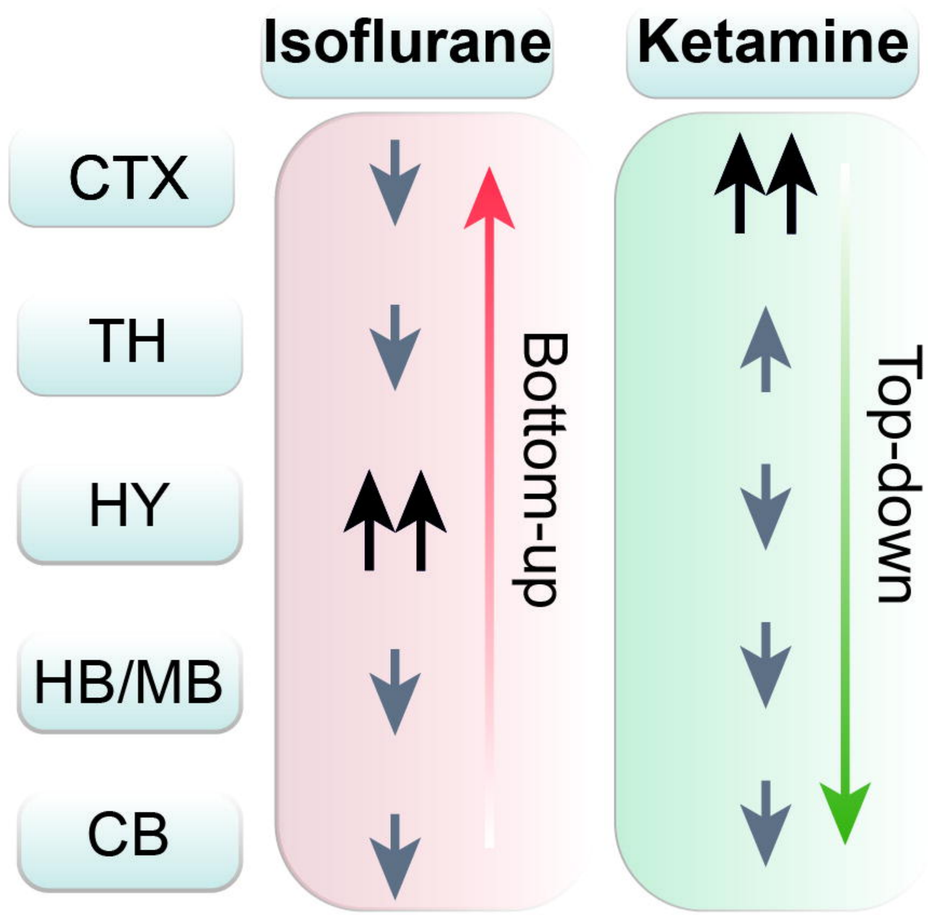

B

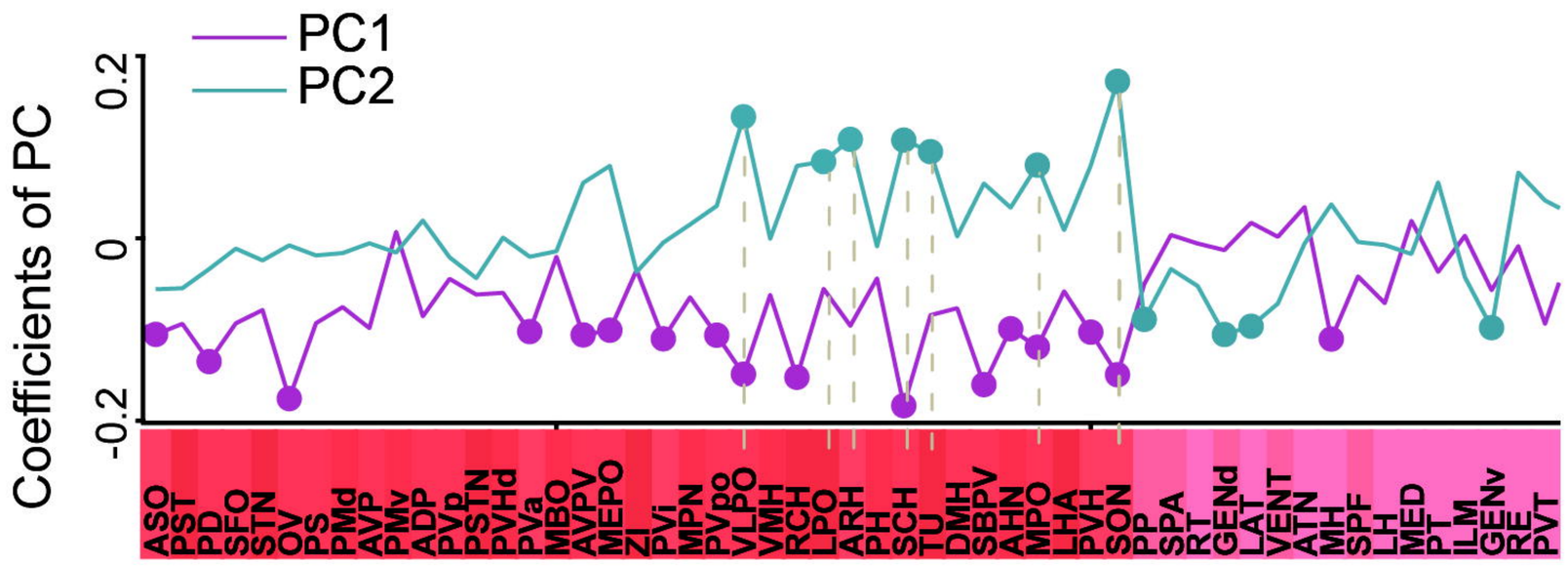

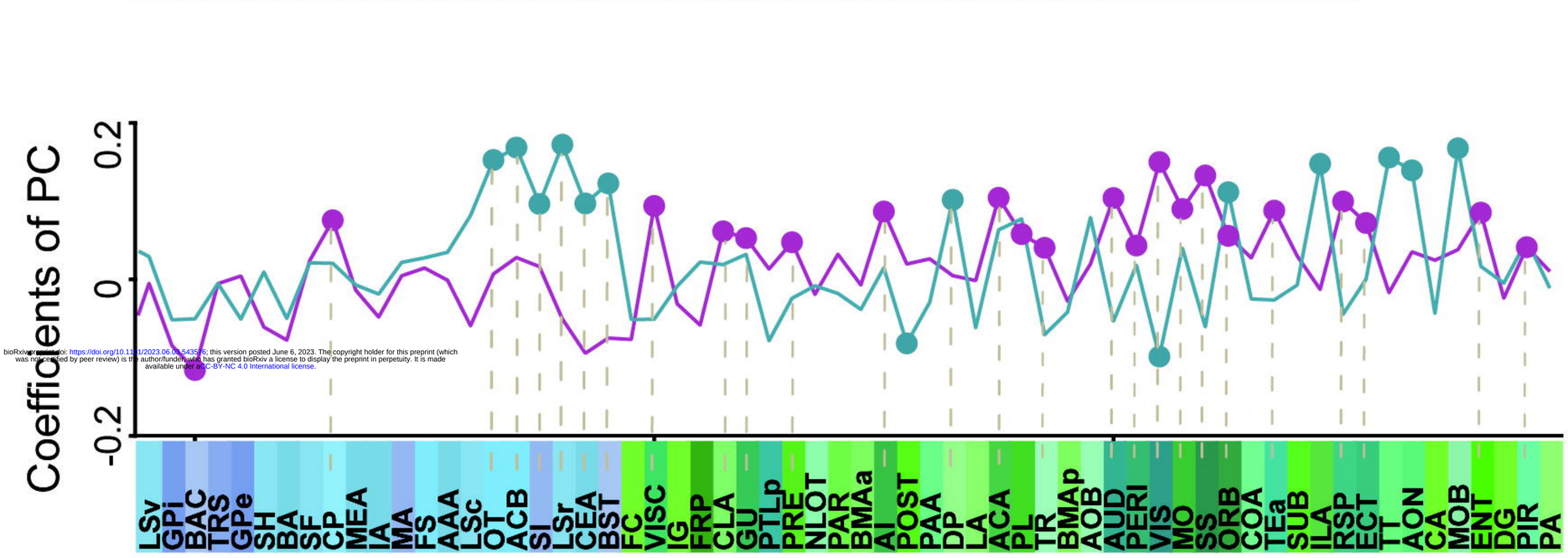

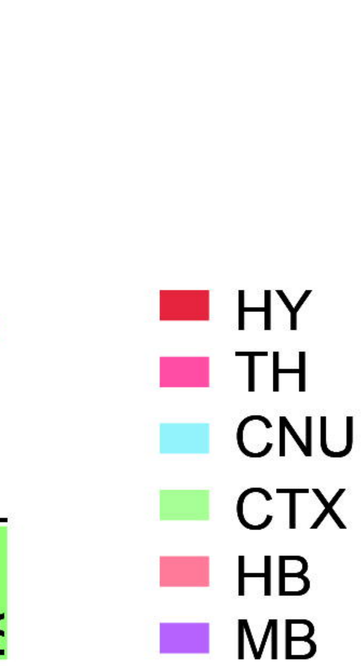

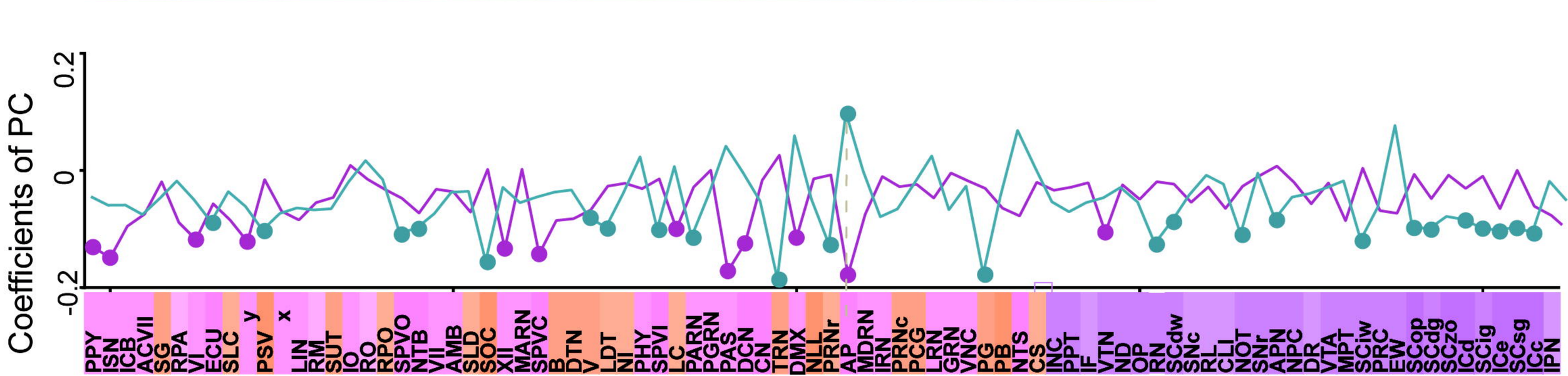

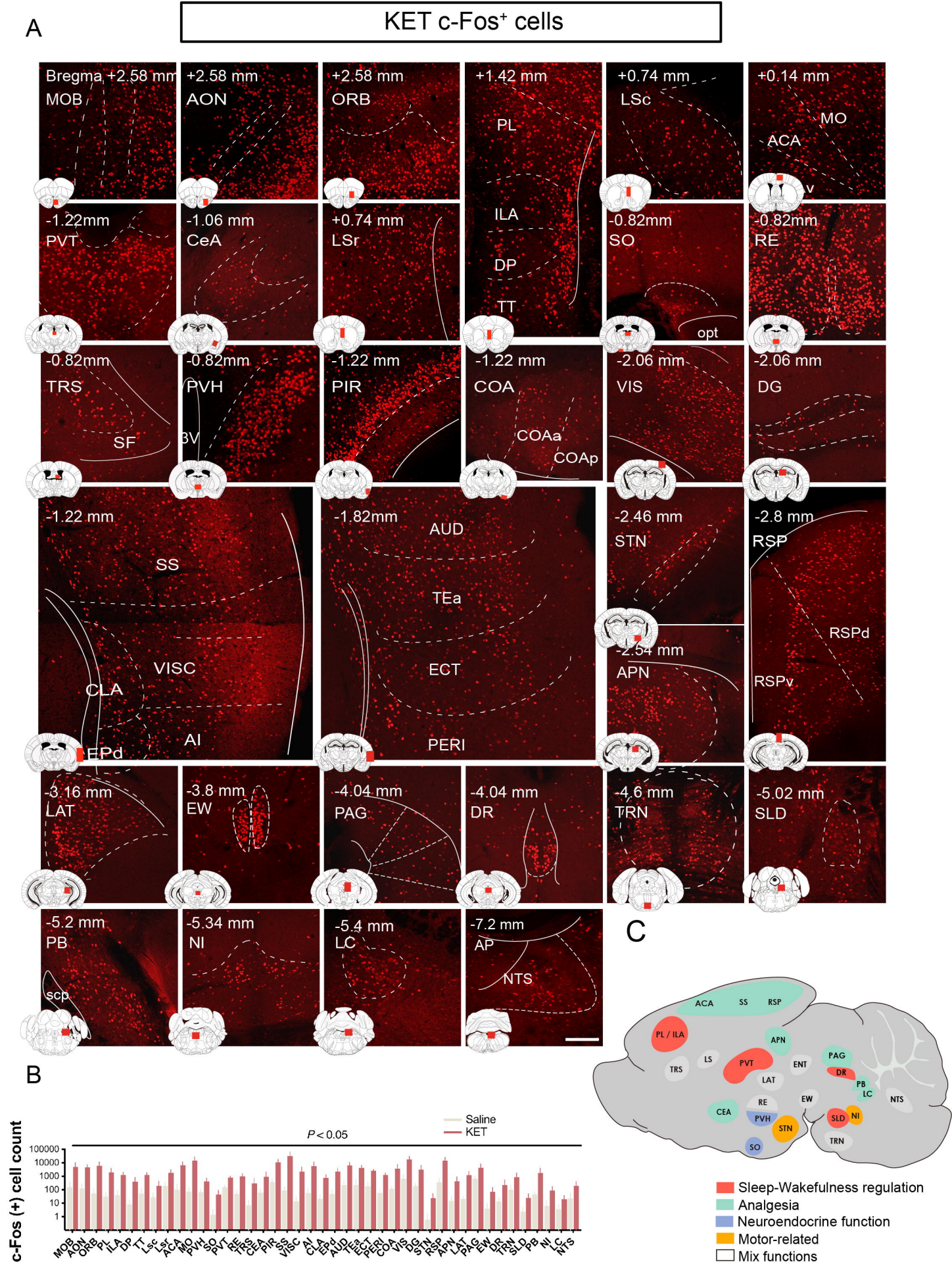
A
KET c-Fos⁺ cells
Bregma +2.58 mm
MOB
+2.58 mm
AON
+2.58 mm
ORB
+1.42 mm
PL
ILA
DP
TT
+0.74 mm
LSc
+0.14 mm
MO
ACA
v
-1.22mm
PVT
-1.06 mm
CeA
+0.74 mm
LSr
-0.82mm
SO
opt
-0.82mm
RE
-0.82mm
TRS
SF
-0.82mm
PVH
3V
-1.22 mm
PIR
-1.22 mm
COA
COAa
COAp
-2.06 mm
VIS
-2.06 mm
DG
-1.22 mm
SS
VISC
CLA
AI
EPd
-1.82mm
AUD
TEa
ECT
PERI
-2.46 mm
STN
-2.54 mm
APN
-2.8 mm
RSP
RSPd
RSPv
-3.16 mm
LAT
-3.8 mm
EW
-4.04 mm
PAG
-4.04 mm
DR
-4.6 mm
TRN
-5.02 mm
SLD
-5.2 mm
PB
scp
-5.34 mm
NI
-5.4 mm
LC
-7.2 mm
AP
NTS
B
Saline
KET
P < 0.05
c-Fos (+) cell count
100000
10000
1000
100
10
1
MOB AON ORB PL ILA DP TT LSc LSr ACA MO PVH SO PVT RE TRS CEA PIR SS VISC AI CLA EPd AUD TEa ECT PERI COA VIS DG STN RSP APN LAT PAG EW DR TRN SLD PB NI LC NTS
C
ACA
SS
RSP
PL / ILA
APN
LS
TRS
PVT
ENT
PAG
DR
LAT
PB
LC
NTS
RE
EW
CEA
PVH
SLD
NI
STN
TRN
SO
Sleep-Wakefulness regulation
Analgesia
Neuroendocrine function
Motor-related
Mix functions

A

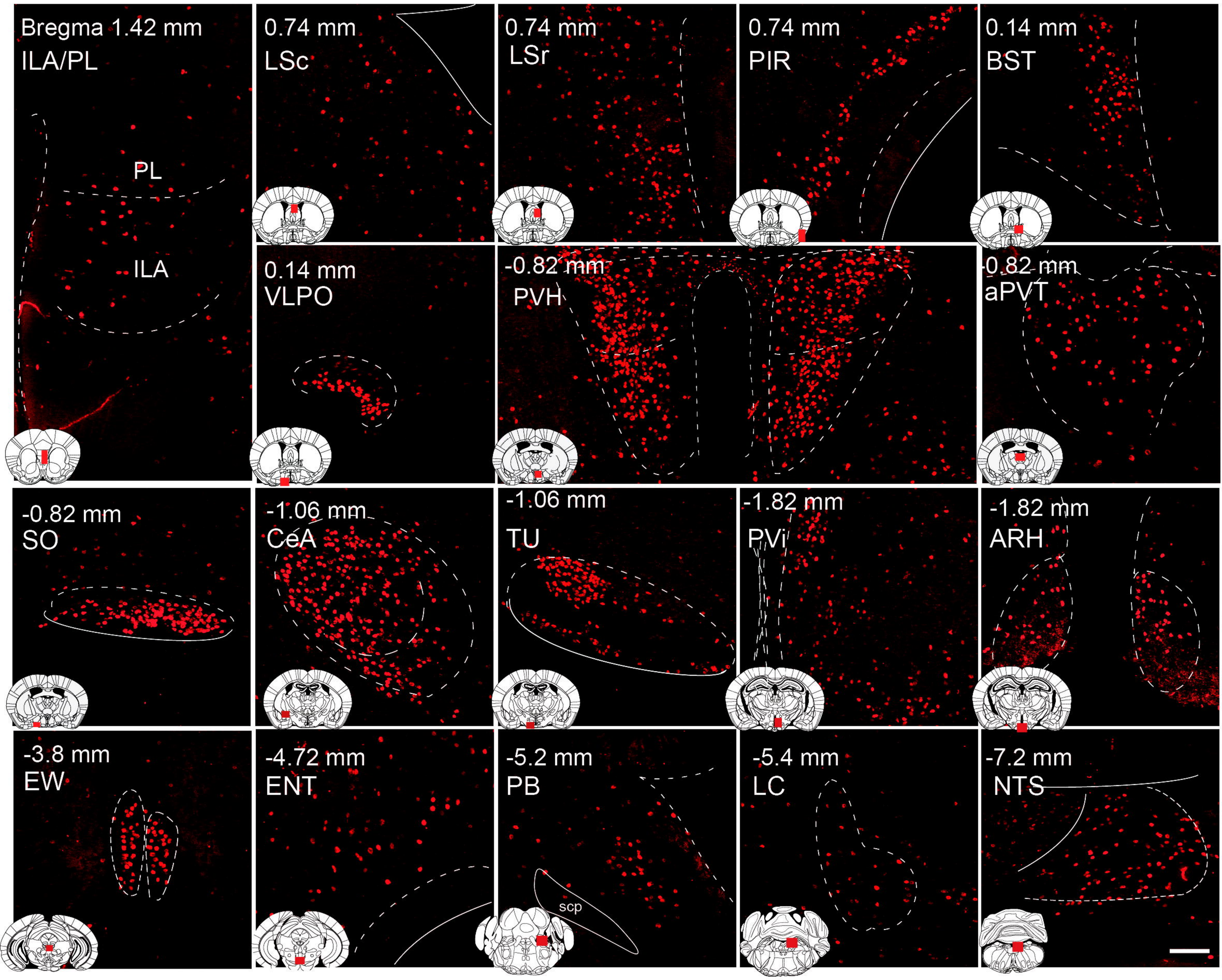

B

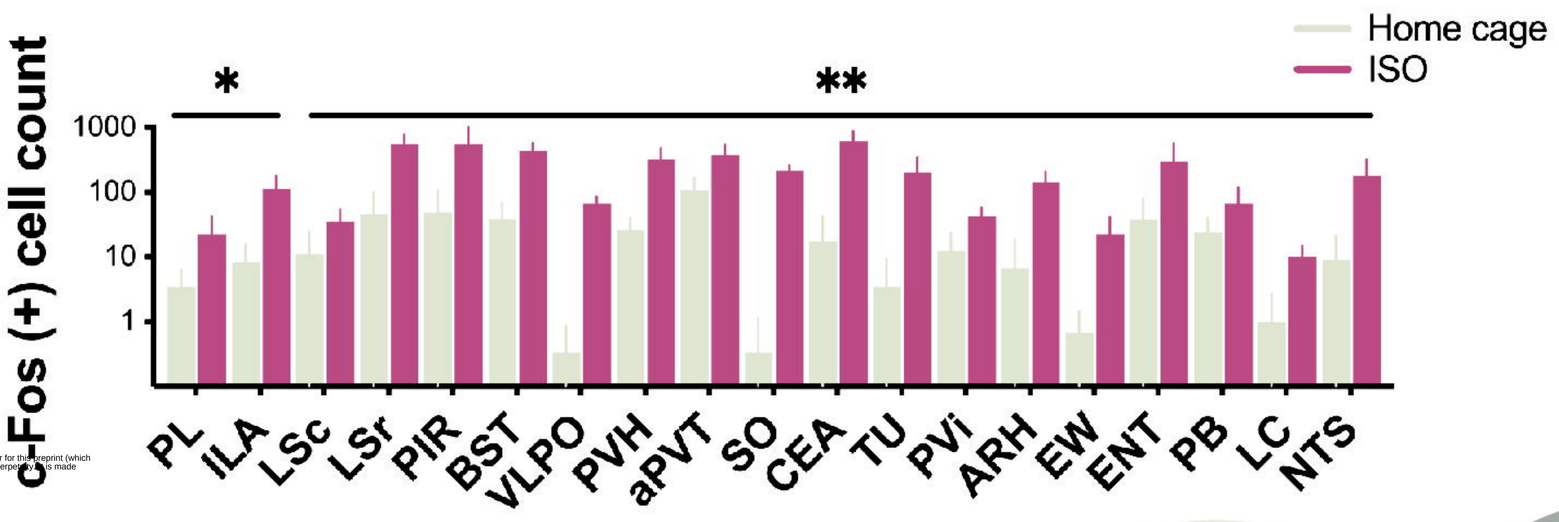

C

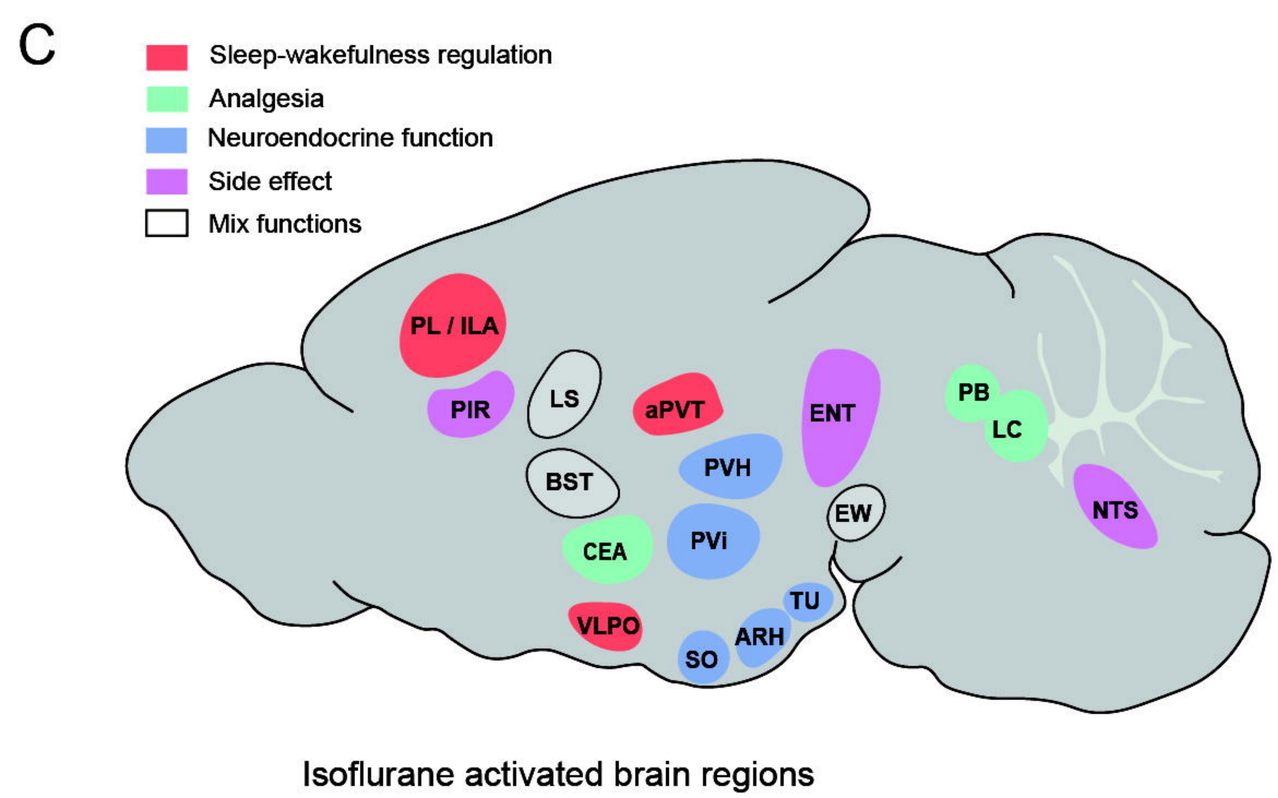

D

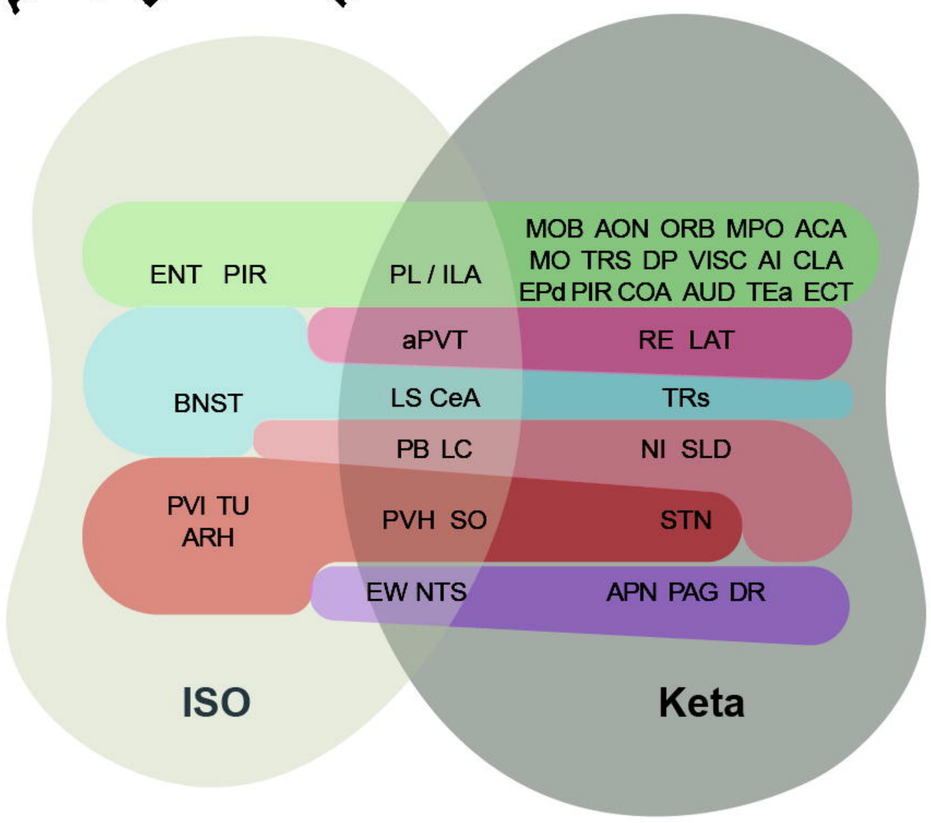

A

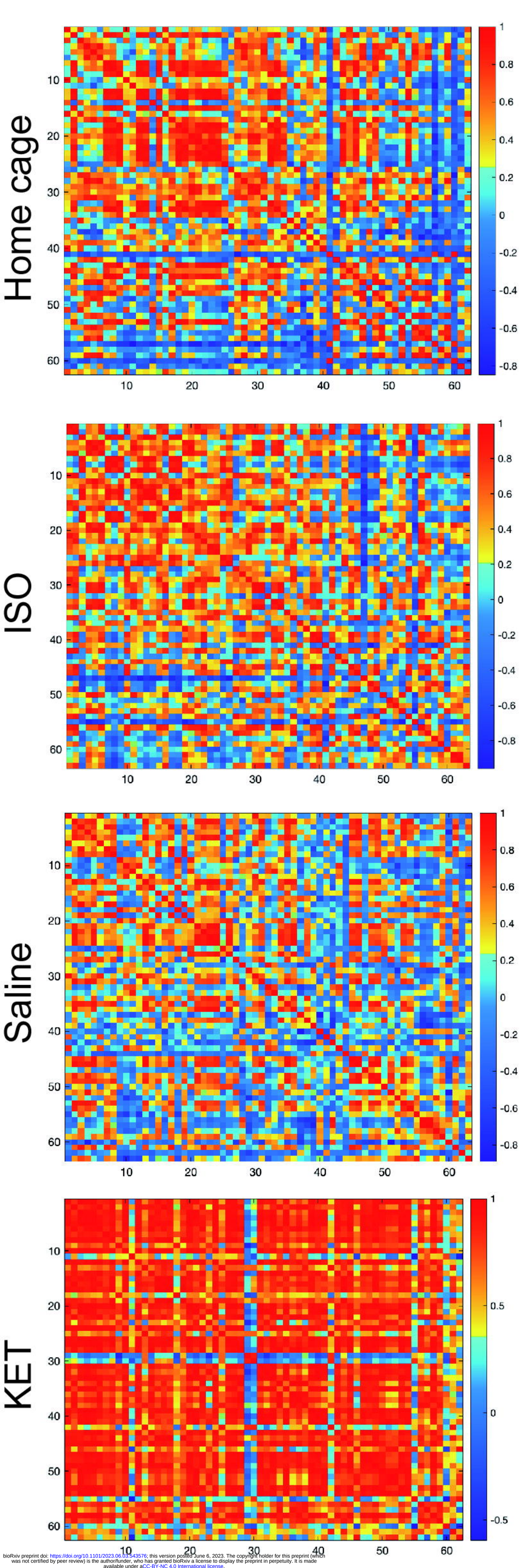

B

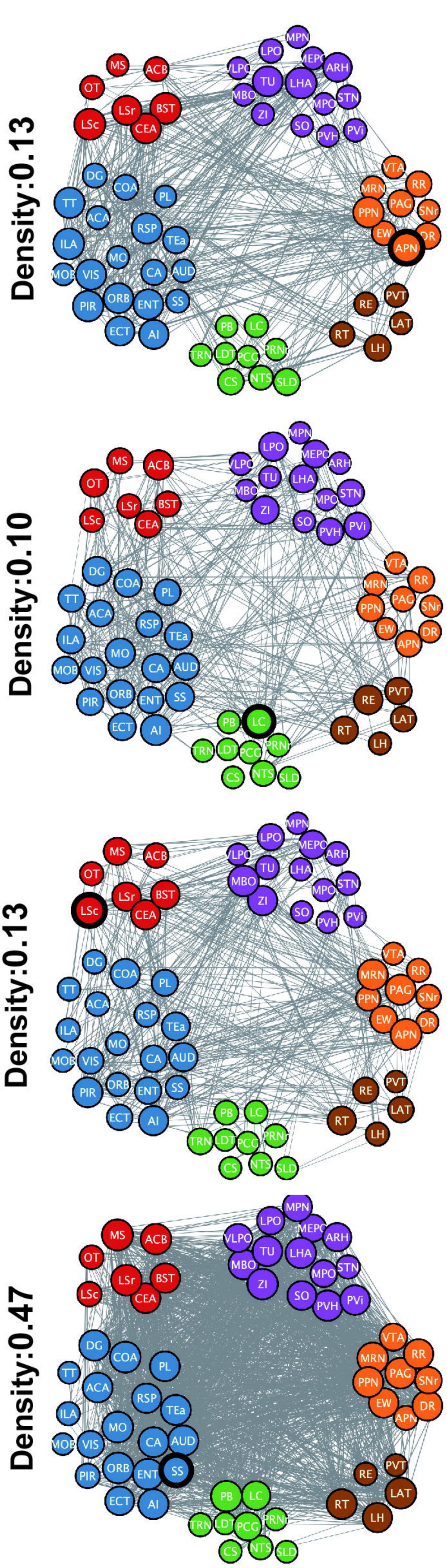

C

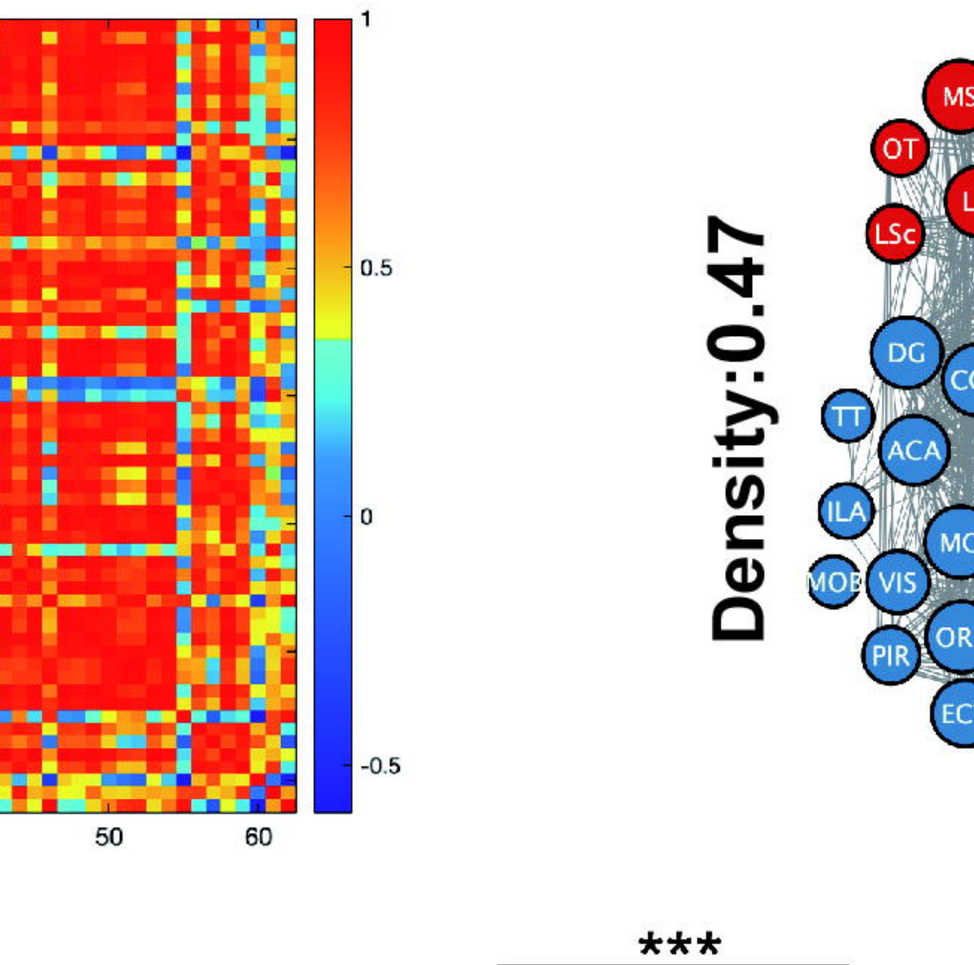

A

Home Cage

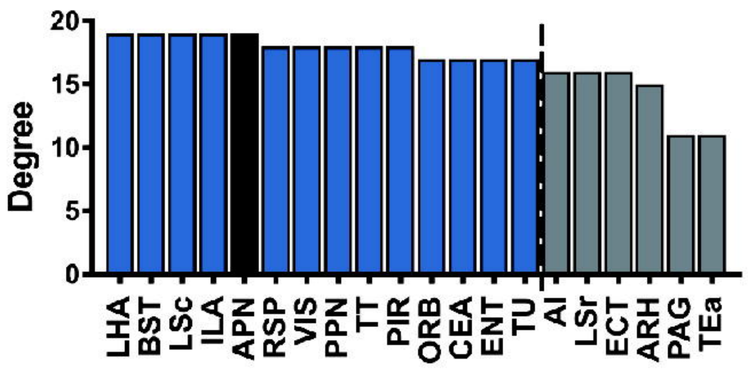

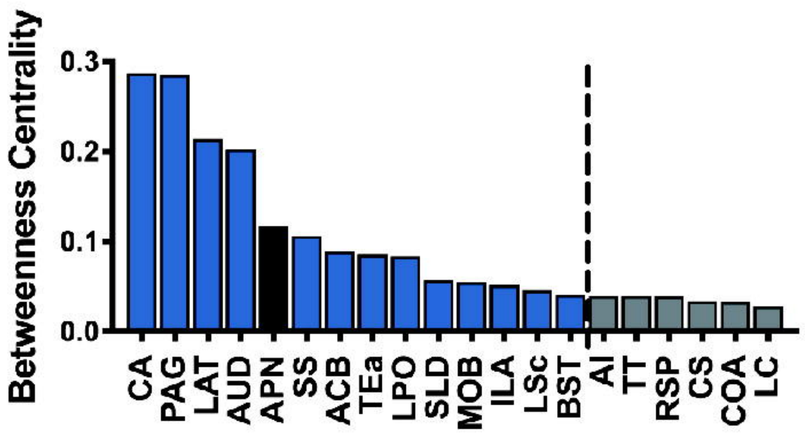

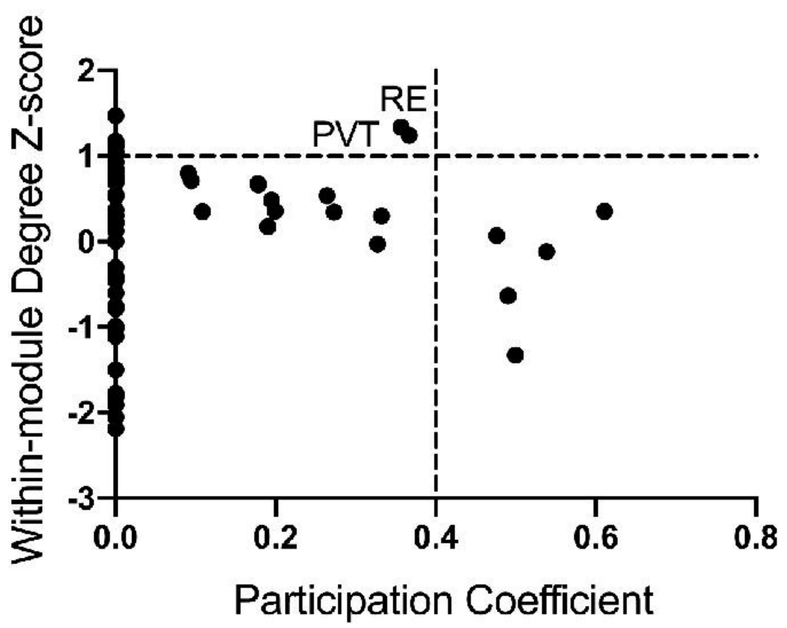

B

ISO

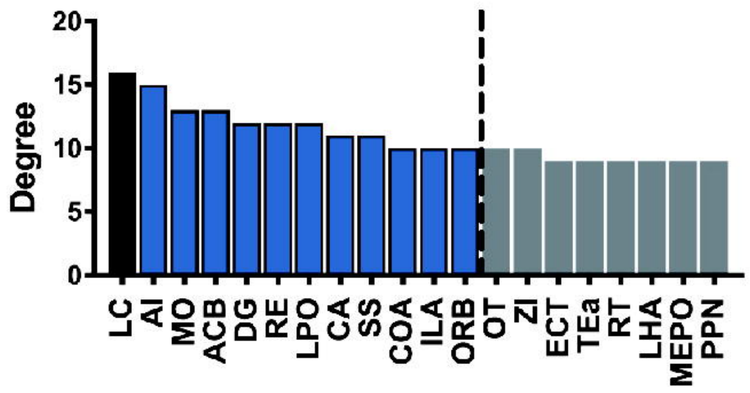

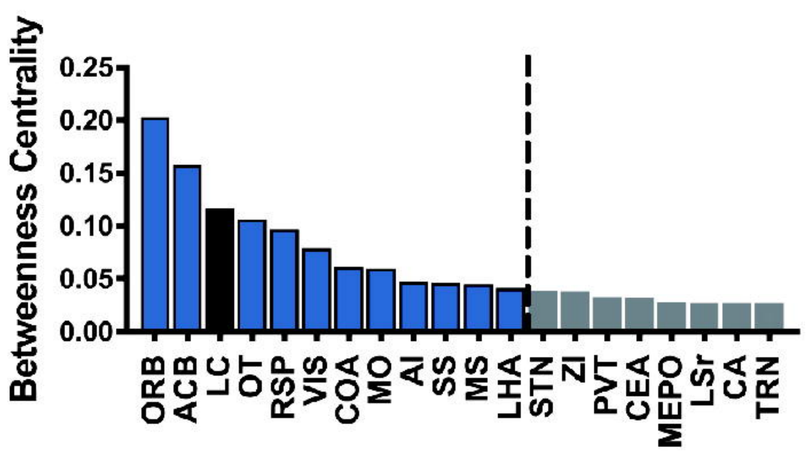

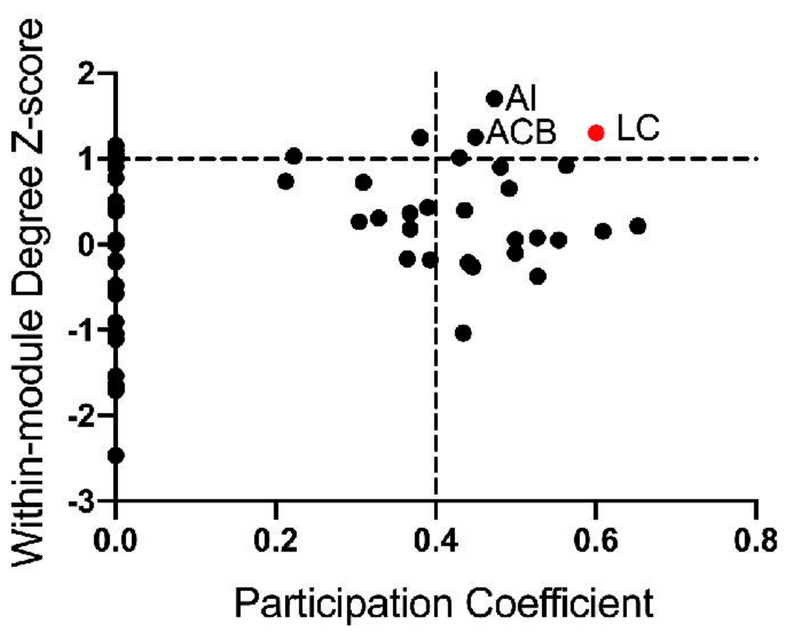

C

Saline

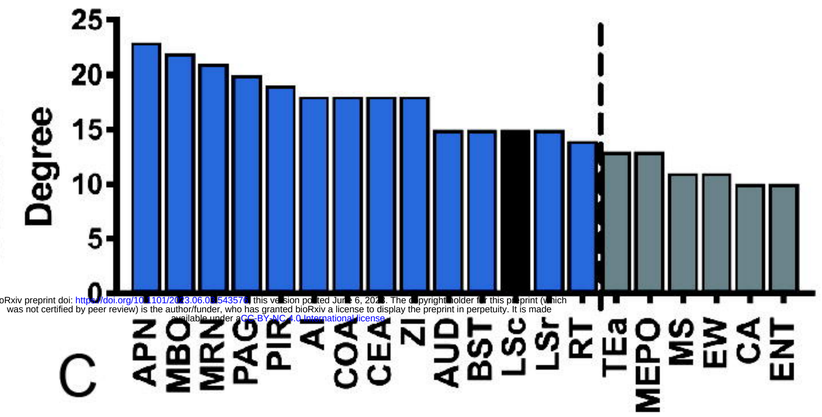

C

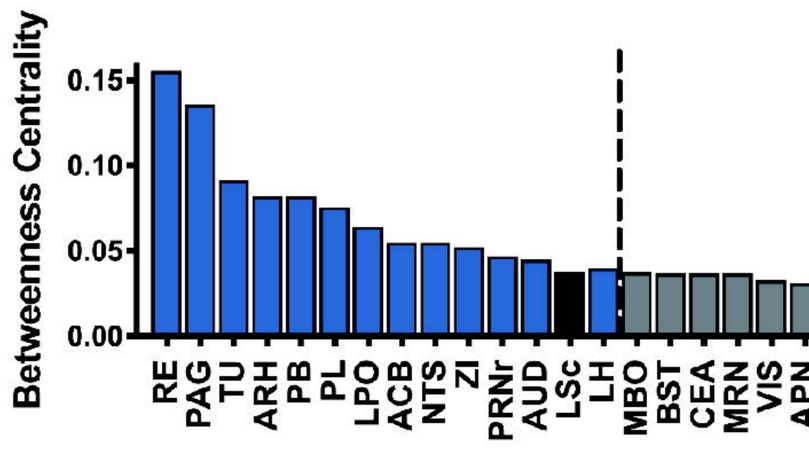

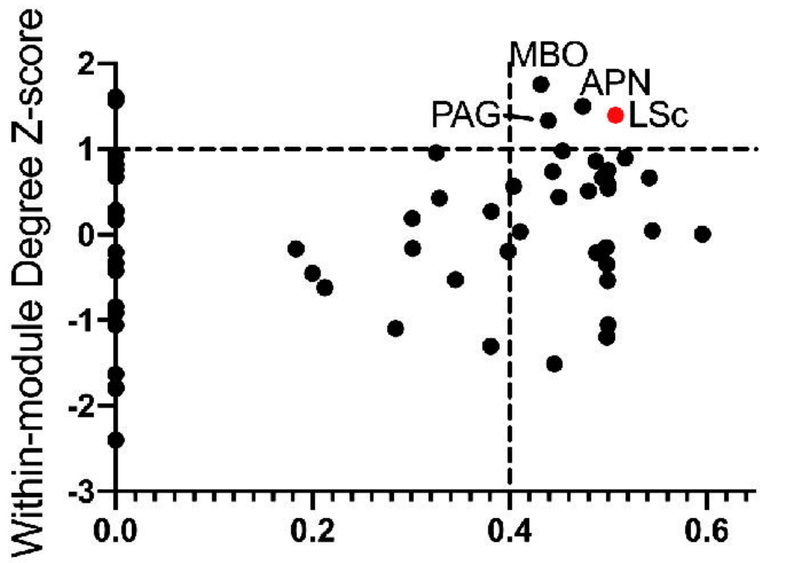

D

KET

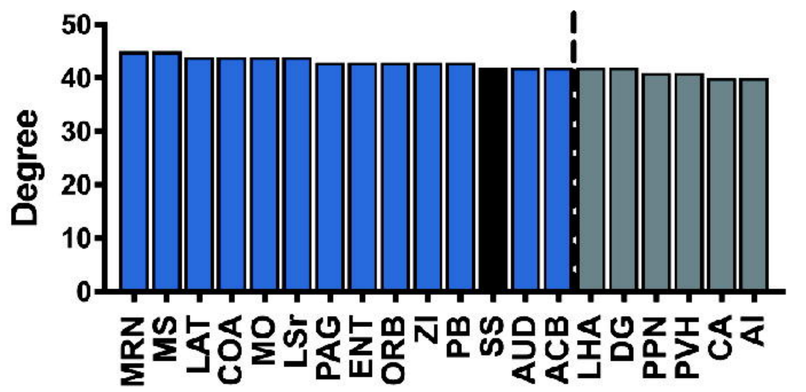

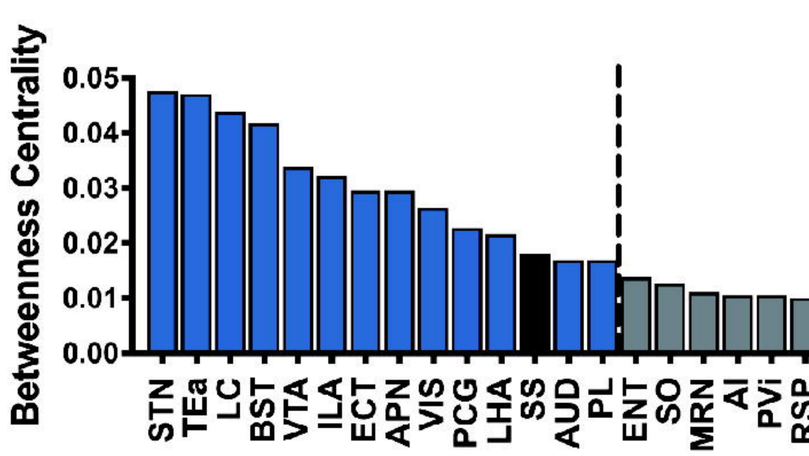

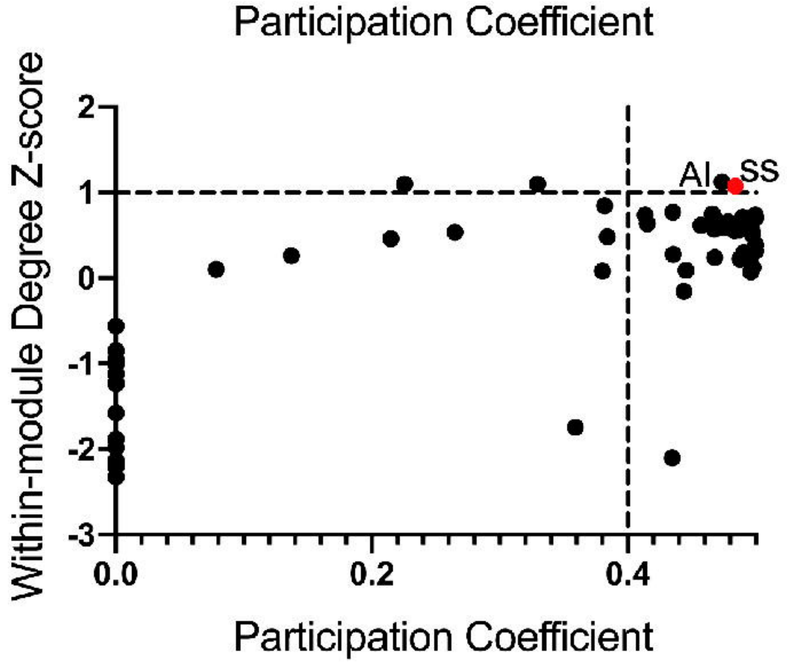

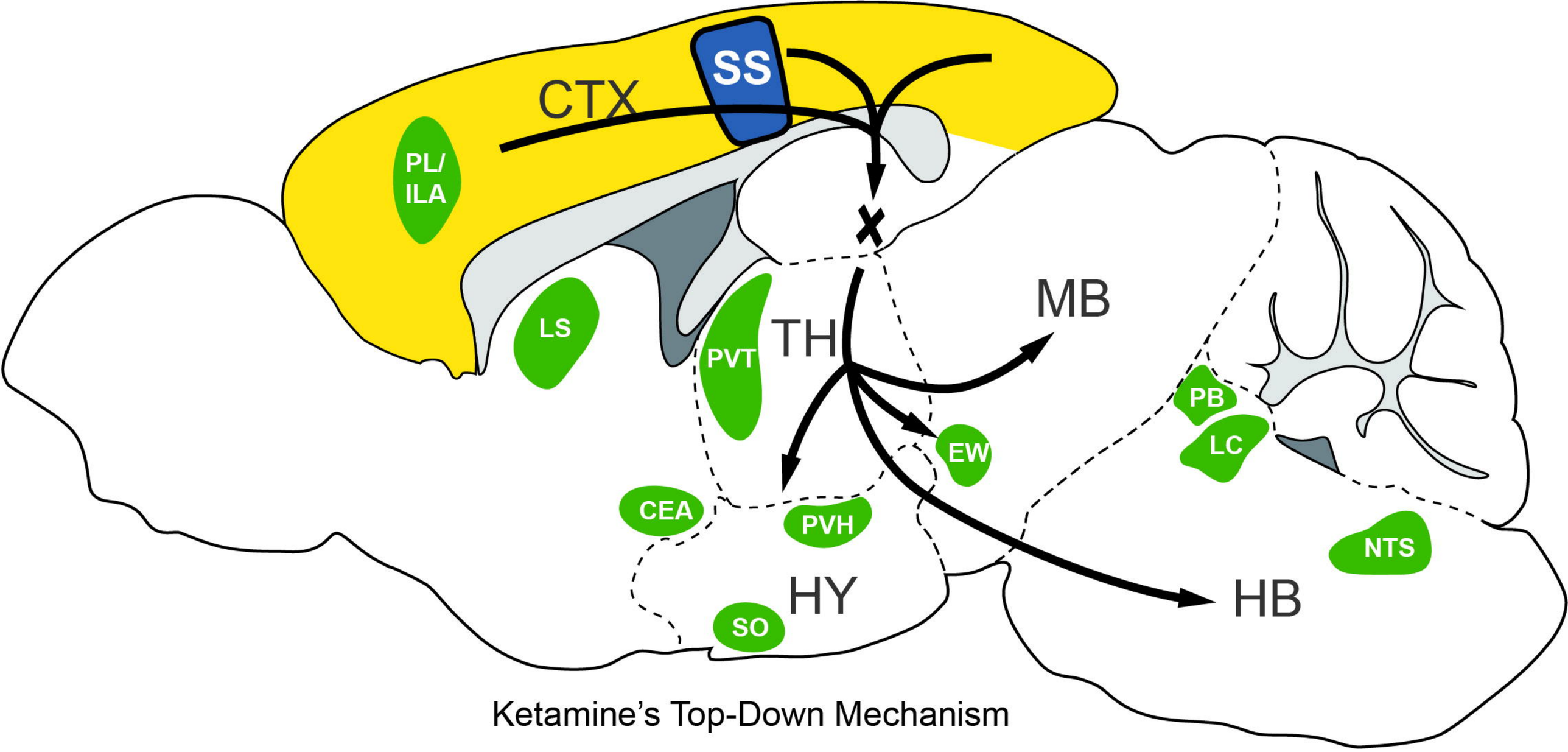

Ketamine's Top-Down Mechanism

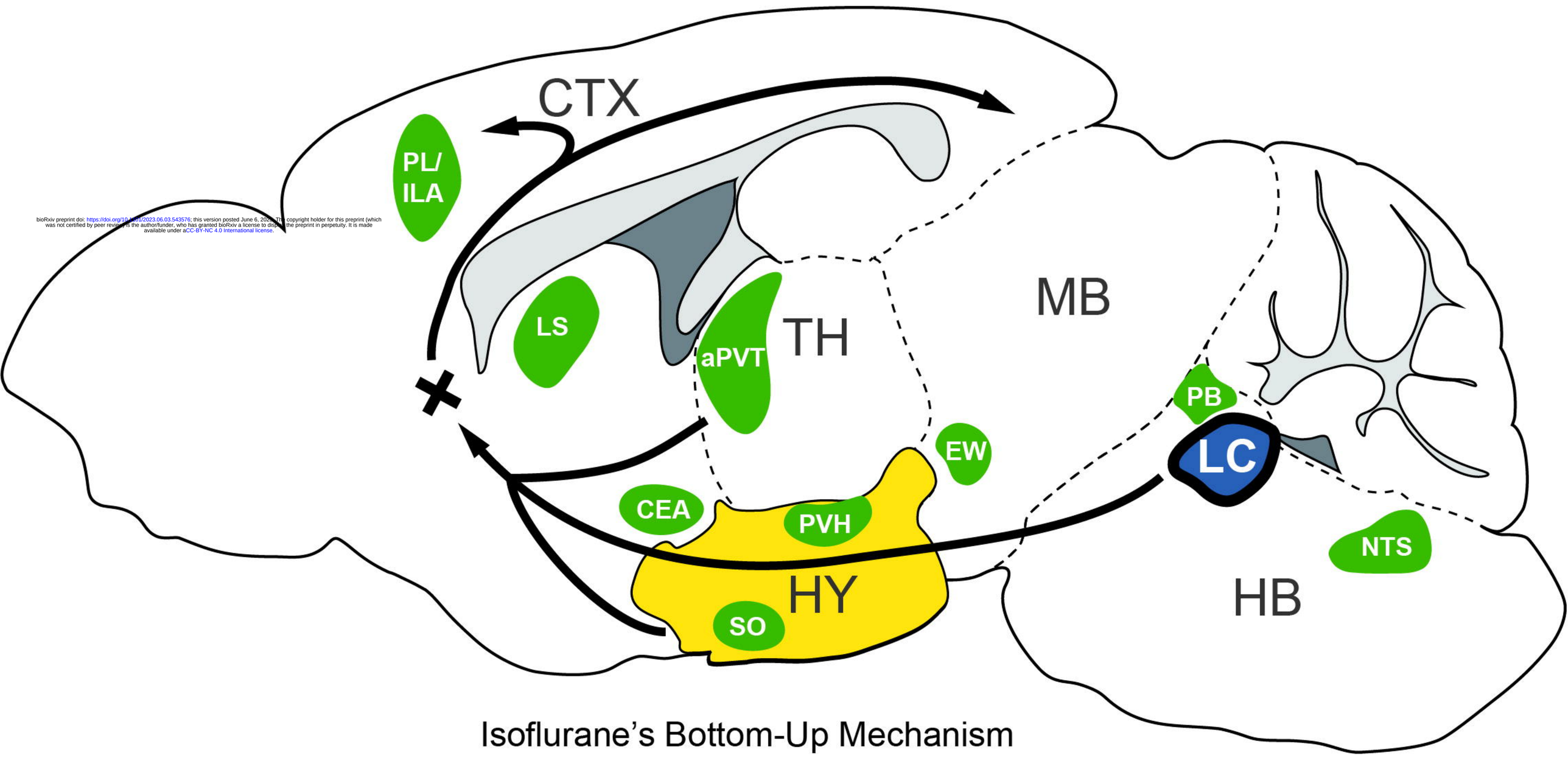

Isoflurane's Bottom-Up Mechanism